APPROXIMATING DISPERSIVE MECHANISMS USING THE DEBYE MODEL WITH DISTRIBUTED DIELECTRIC PARAMETERS

KAREN BARRESE AND NEEL CHUGH

ADVISOR: NATHAN GIBSON
OREGON STATE UNIVERSITY

ABSTRACT. The Cole-Cole model is known to accurately describe the dielectric response to a pulse over a wide range of frequencies. The model, however, does not lend itself easily to the Finite Difference Time Domain (FDTD) method, as it requires the computation of fractional-order derivatives and a more complicated implementation. Researchers have instead often used the multi-pole Debye model, which is characterized by the same dielectric parameters as the Cole-Cole model, but has less accuracy in describing the dielectric response. In this paper, we seek to reconcile the difficulty of implementing the Cole-Cole model by presenting an approximation of dispersive mechanisms and the Cole-Cole model using distributions of parameters within the Debye model.

1. INTRODUCTION

Over the past century, researchers have made many strides toward better understanding the Debye model and Debye mechanisms. The Debye model is commonly defined as a physically derived model of dipolar relaxation. On the other hand, less is known about the multiple dispersive mechanisms approximated by the Cole-Cole model. While the Cole-Cole model is simply a heuristic generalization of the Debye model, understanding the mechanisms it describes is of importance because of the model's great accuracy in matching experimental observations. Another divide between the two models arises when looking at their dielectric response functions (DRF). Due to the complex nature of the Cole-Cole model's DRF, computational and numerical methods that attempt to simulate the Cole-Cole model require the need to approximate fractional-order derivatives [4]. The Debye model, alternatively, can be implemented rather easily. In this paper, we propose ways in which the Debye model can be adjusted to better approximate both the Cole-Cole model and true data.

We begin by displaying background material related to how we can simulate electromagnetic waves moving through a dielectric. First, the Finite-Difference Time Domain (FDTD) method is thoroughly explained and used to derive expressions for the electric field and polarization in one-dimension. After this, we present a new version of the standard FDTD procedure to allow for distributions of dielectric parameters in the Debye model along with multiple polarization factors. We proceed to formulate an inverse problem to determine the distribution parameters that make the distributed Debye model as accurate as possible. Dry skin tissue is used as an example of a material for which such an inverse problem is possible.

To display the efficacy of using a distribution of parameters, we will perform forward simulations using an ultra-wideband (UWB) electromagnetic pulse through a dielectric with the parameters of dry skin using our revised FDTD model. A UWB pulse, which is defined over a wide range

Date: August 15, 2008.

This work was done during the Summer 2008 REU program in Mathematics at Oregon State University.

of frequencies, is used to determine how well the Debye model with distributed dielectric parameters describes a material with a frequency dependent dielectric response. The forward simulations with dielectric parameter distributions could also be utilized in a standard time domain inverse problem to recover dielectric parameters, however that is not the object of this effort. We provide a general form of the inverse problem and forward simulations, so that they can be extended to other human tissue samples and dielectric materials.

2. BACKGROUND

Since we are interested in observing electromagnetic waves generated by a pulse, we must start with the system of Maxwell's equations, as found in [7], which are

$$\frac{\partial \mathbf{D}}{\partial t} + \mathbf{J} = \nabla \times \mathbf{H} \tag{1}$$

$$\frac{\partial \mathbf{B}}{\partial t} = -\nabla \times \mathbf{E} \tag{2}$$

$$\nabla \cdot \mathbf{D} = \rho \tag{3}$$

$$\nabla \cdot \mathbf{B} = 0. \tag{4}$$

Additional vital equations, the constitutive laws, are

$$\mathbf{D} = \varepsilon \mathbf{E} + \mathbf{P} \tag{5}$$

$$\mathbf{B} = \mu \mathbf{H} + \mathbf{M} \tag{6}$$

$$\mathbf{J} = \sigma \mathbf{E} + \mathbf{J}_s, \tag{7}$$

where $\varepsilon = \varepsilon_0 \varepsilon_\infty$. The electric and magnetic fields are represented by $\mathbf{E}$ and $\mathbf{H}$, respectively, $\mathbf{D}$ and $\mathbf{B}$ represent the electric and magnetic flux densities, respectively, $\mathbf{M}$ is the magnetization, and $\mathbf{P}$ is the polarization. The two currents are give by the conduction current density, $\mathbf{J}$, and the source current density, $\mathbf{J}_s$. The scalar quantities are ρ, the density of free electric charges unaccounted for in the electric polarization; ε_0, the electric permittivity of free space; ε_∞, the electric permittivity in the limit of infinite frequencies; μ, the magnetic permeability; and σ, the electric conductivity. For future reference, we also will be considering ε_s, the static electric permittivity i.e. the limit of zero frequency. The dielectric parameters describe the polarization $\mathbf{P}$. The polarization, written in the convolution form, is

$$\mathbf{P}(t,\mathbf{x}) = g \star \mathbf{E}(t,\mathbf{x}) = \int_0^t g(t-s,\mathbf{x};\nu)\mathbf{E}(s,\mathbf{x})ds, \tag{8}$$

where $g(t,\mathbf{x})$ and ν is a set of dielectric parameters is a dielectric response function (DRF). The DRF for a Debye Medium is

$$g(t,\mathbf{x}) = \frac{\varepsilon_0(\varepsilon_s - \varepsilon_\infty)}{\tau} e^{-t/\tau} \tag{9}$$

with $\nu = \{\varepsilon_s, \varepsilon_\infty, \tau\}$. Polarization in (8) defined by (9) can be shown to be equivalent to the solution of the ordinary differential equation,

$$\tau \dot{\mathbf{P}} + \mathbf{P} = \varepsilon_0 \varepsilon_d \mathbf{E}, \tag{10}$$

where $\varepsilon_d = \varepsilon_s - \varepsilon_\infty$.

To simulate the waves, we must know how the electromagnetic fields behave in time and space. This is uniquely determined by Maxwell's curl equations, with appropriate initial and boundary conditions, and substitutions from Equations 5 and 6. Making the assumption that there is no magnetization, we have

$$\varepsilon\frac{\partial \mathbf{E}}{\partial t} = \nabla\times\mathbf{H} - \mathbf{J} - \frac{\partial \mathbf{P}}{\partial t} = \nabla\times\mathbf{H} - \sigma\mathbf{E} - \frac{\partial \mathbf{P}}{\partial t}. \tag{11}$$

$$\mu\frac{\partial \mathbf{H}}{\partial t} = -\nabla\times\mathbf{E}. \tag{12}$$

For our purposes, we will simplify the problem to one-dimensional space, similar to the approach in [9], with the assumption that the electric field oscillates only in the xz-plane and propagates in the z direction. This leaves us with only two relevant equations for the one-dimensional problem, which are

$$\varepsilon\frac{\partial E_x}{\partial t} = -\frac{\partial H_y}{\partial z} - \sigma E_x - \frac{\partial P_x}{\partial t}. \tag{13}$$

$$\mu\frac{\partial H_y}{\partial t} = -\frac{\partial E_x}{\partial z}. \tag{14}$$

From now on, we will now let $E = E_x, H = H_y$ and $P = P_x$.

3. The FDTD Method

Using Maxwell's equations, it is apparent that one can solve for both the electric and magnetic fields at different points in time and space, when given necessary boundary conditions. One method to solve these equations is the Finite Difference Time Domain (FDTD) method. This method uses a staggered grid with **E** on integer points in space and half-steps in time and **H** on half-steps in space and integer points in time. A detailed explanation of this can be found in [9].

To use the FDTD method, we need to be able to approximate both E_x and H_y at the appropriate grid points. This can be done using a central difference approximation for both the time and spacial derivatives. Applying the central difference approximation, as used in [9], (13) can be written as

$$\frac{E_k^{n+\frac{1}{2}} - E_k^{n-\frac{1}{2}}}{\Delta t} = -\frac{1}{\varepsilon}\frac{H_{k+\frac{1}{2}}^n - H_{k-\frac{1}{2}}^n}{\Delta z} - \frac{\sigma}{\varepsilon}\frac{E_k^{n+\frac{1}{2}} + E_k^{n-\frac{1}{2}}}{2} - \frac{1}{\varepsilon}\frac{P_k^{n+\frac{1}{2}} - P_k^{n-\frac{1}{2}}}{\Delta t}. \tag{15}$$

Since the electric field updates prior to the polarization, we must find an expression for $P_k^{n+\frac{1}{2}}$. From (10), once again using the central difference approximation, we have

$$\tau\frac{P_k^{n+\frac{1}{2}} - P_k^{n-\frac{1}{2}}}{\Delta t} + \frac{P_k^{n+\frac{1}{2}} + P_k^{n-\frac{1}{2}}}{2} = \varepsilon_0\varepsilon_d\frac{E_k^{n+\frac{1}{2}} + E_k^{n-\frac{1}{2}}}{2}. \tag{16}$$

Solving for $P_k^{n+\frac{1}{2}}$, we see

$$P_k^{n+\frac{1}{2}} = \frac{\Delta t\varepsilon_0\varepsilon_d\left[E_k^{n+\frac{1}{2}} + E_k^{n-\frac{1}{2}}\right] + (2\tau - \Delta t)P_k^{n-\frac{1}{2}}}{2\tau + \Delta t}. \tag{17}$$

Substituting the expression for $P_k^{n+\frac{1}{2}}$ into (15), we have

$$\frac{E_k^{n+\frac{1}{2}}-E_k^{n-\frac{1}{2}}}{\Delta t}=-\frac{1}{\varepsilon}\frac{H_{k+\frac{1}{2}}^n-H_{k-\frac{1}{2}}^n}{\Delta z}-\frac{\sigma}{\varepsilon}\frac{E_k^{n+\frac{1}{2}}+E_k^{n-\frac{1}{2}}}{2}-\frac{1}{\varepsilon}\frac{\frac{\Delta t\varepsilon_0\varepsilon_d}{2\tau+\Delta t}\left[E_k^{n+\frac{1}{2}}+E_k^{n-\frac{1}{2}}\right]+\frac{2\tau-\Delta t}{2\tau+\Delta t}P_k^{n-\frac{1}{2}}-P_k^{n-\frac{1}{2}}}{\Delta t}$$

Arranging the $E_k^{n+\frac{1}{2}}$ terms together in the process of solving for $E_k^{n+\frac{1}{2}}$, we see

$$E_k^{n+\frac{1}{2}}\left[1+\frac{\sigma\Delta t}{2\varepsilon}+\frac{\Delta t\varepsilon_d}{\varepsilon_\infty(2\tau+\Delta t)}\right]=-\frac{\Delta t}{\varepsilon\Delta z}\left[H_{k+\frac{1}{2}}^n-H_{k-\frac{1}{2}}^n\right]+E_k^{n-\frac{1}{2}}\left[1-\frac{\sigma\Delta t}{2\varepsilon}-\frac{\Delta t\varepsilon_d}{\varepsilon_\infty(2\tau+\Delta t)}\right]+\frac{2\Delta t}{\varepsilon(2\tau+\Delta t)}P_k^{n-\frac{1}{2}}.$$

We will define $\theta=-\frac{\Delta t}{\varepsilon\Delta z}$ and the loss term $\delta=\frac{\sigma\Delta t}{2\varepsilon}+\frac{\Delta t\varepsilon_d}{\varepsilon_\infty(2\tau+\Delta t)}$, which gives us

$$E_k^{n+\frac{1}{2}}=\frac{\theta}{1+\delta}\left[H_{k+\frac{1}{2}}^n-H_{k-\frac{1}{2}}^n\right]+\frac{1-\delta}{1+\delta}E_k^{n-\frac{1}{2}}+\frac{2\Delta t}{\varepsilon(2\tau+\Delta t)(1+\delta)}P_k^{n-\frac{1}{2}}. \tag{18}$$

This can be viewed as a variation of Equation (2.21a) used by Sullivan [9]. We can similarly find an expression for the magnetic field

$$H_{k+\frac{1}{2}}^{n+1}=-\frac{\Delta t}{\mu\Delta z}\left[E_k^{n+\frac{1}{2}}-E_k^{n-\frac{1}{2}}\right]+H_{k+\frac{1}{2}}^n. \tag{19}$$

These are explicit update rules that requires no past history to be stored.

4. Distributions of Dielectric Parameters and Multiple Polarizations

4.1. **Uniform Distribution for τ.** Since we are looking to simulate the Debye model using distributions of parameters, we first must restate our polarization term to include such distributions. We begin by applying a distribution to the dielectric parameter τ. We build upon the framework used by Banks and Gibson [2], where equation (15) stated

$$P(t,z)=\int_{\tau_a}^{\tau_b}\mathcal{P}(t,z;\tau)dF(\tau)=\frac{1}{\tau_b-\tau_a}\int_{\tau_a}^{\tau_b}\mathcal{P}(t,z;\tau)d\tau, \tag{20}$$

since $dF(\tau)=\frac{1}{\tau_b-\tau_a}d\tau$ for a uniform distribution. Banks and Gibson discuss the difficulty of arriving at an analytical solution for such an integral and the need to use the Composite Simpson's rule approximation [2]. Using this rule, we see that polarization can be approximated as $P(t,z)=\sum_{i=0}^{\ell}\alpha_i\mathcal{P}(t,z;\tau_i)$, where $\alpha_i=\frac{c_i^\ell}{\ell}$ and τ is modeled by a uniform distribution. This approximation holds when ℓ is even and

$$c_i^\ell=\begin{cases}\frac{1}{3} & \text{if } i=0 \text{ or } i=\ell\\ \frac{4}{3} & \text{else if } i \text{ odd}\\ \frac{2}{3} & \text{else if } i \text{ even}\end{cases}.$$

Using this substitute for polarization, (13) can now be written as

$$\varepsilon\frac{\partial E}{\partial t}=-\frac{\partial H}{\partial z}-\sigma E-\sum_{i=0}^{\ell}\alpha_i\frac{\partial\mathcal{P}_i}{\partial t}, \tag{21}$$

where $\mathcal{P}_i = \mathcal{P}(t,z;\tau_i)$. Applying FDTD, we find

$$\sum_{i=0}^{\ell} \alpha_i \frac{\partial \mathcal{P}_i}{\partial t} \approx \sum_{i=0}^{\ell} \alpha_i \frac{[(\mathcal{P}_i)_k^{n+\frac{1}{2}} - (\mathcal{P}_i)_k^{n-\frac{1}{2}}]}{\Delta t}.$$

We can use this polarization, which includes a uniformly distributed τ, to update Equations (17) and (18), which are now written as

$$(\mathcal{P}_i)_k^{n+\frac{1}{2}} = \frac{\Delta t \varepsilon_0 \varepsilon_d [E_k^{n+\frac{1}{2}} + E_k^{n-\frac{1}{2}}] + (2\tau_i - \Delta t)(\mathcal{P}_i)_k^{n-\frac{1}{2}}}{2\tau_i + \Delta t} \tag{22}$$

$$E_k^{n+\frac{1}{2}} = \frac{\theta}{1+\delta}[H_{k+\frac{1}{2}}^n - H_{k-\frac{1}{2}}^n] + \frac{1-\delta}{1+\delta} E_k^{n-\frac{1}{2}} + \sum_{i=0}^{\ell} \frac{2\Delta t \alpha_i}{\varepsilon(2\tau_i + \Delta t)(1+\delta)} (\mathcal{P}_i)_k^{n-\frac{1}{2}}, \tag{23}$$

where $\delta = \frac{\sigma \Delta t}{2\varepsilon} + \sum_{i=0}^{\ell} \alpha_i \frac{\Delta t \varepsilon_d}{\varepsilon_\infty (2\tau_i + \Delta t)}$.

4.2. **Uniform Distribution for ε_d.** The above shows the electric field and polarization equations with a distribution included only for the parameter τ. We can additionally add in a uniform distribution for the dielectric parameter ε_d, where $\varepsilon_d = \varepsilon_s - \varepsilon_\infty$. Applying the Composite Simpson's approximation for polarization and updating (21), we find that

$$\varepsilon \frac{\partial E}{\partial t} = -\frac{\partial H}{\partial z} - \sigma E - \sum_{j=0}^{\ell} \sum_{i=0}^{\ell} \beta_j \alpha_i \frac{\partial \mathcal{P}_{ij}}{\partial t}, \tag{24}$$

where $\mathcal{P}_{ij} = \mathcal{P}(t,z;\tau_i,\varepsilon_{d_j})$. Once again, using FDTD

$$\sum_{j=0}^{\ell} \sum_{i=0}^{\ell} \beta_j \alpha_i \frac{\partial \mathcal{P}_{ij}}{\partial t} \approx \sum_{j=0}^{\ell} \sum_{i=0}^{\ell} \beta_j \alpha_i \frac{[(\mathcal{P}_{ij})_k^{n+\frac{1}{2}} - (\mathcal{P}_{ij})_k^{n-\frac{1}{2}}]}{\Delta t}.$$

Equations (22) and (23) are amended as follows:

$$(\mathcal{P}_{ij})_k^{n+\frac{1}{2}} = \frac{\Delta t \varepsilon_0 \varepsilon_{d_j} [E_k^{n+\frac{1}{2}} + E_k^{n-\frac{1}{2}}] + (2\tau_i - \Delta t)(\mathcal{P}_{ij})_k^{n-\frac{1}{2}}}{2\tau_i + \Delta t}. \tag{25}$$

$$E_k^{n+\frac{1}{2}} = \frac{\theta}{1+\delta}[H_{k+\frac{1}{2}}^n - H_{k-\frac{1}{2}}^n] + \frac{1-\delta}{1+\delta} E_k^{n-\frac{1}{2}} + \sum_{j=0}^{\ell} \sum_{i=0}^{\ell} \frac{2\Delta t \alpha_i \beta_j}{\varepsilon(2\tau_i + \Delta t)(1+\delta)} (\mathcal{P}_{ij})_k^{n-\frac{1}{2}} \tag{26}$$

where $\delta = \frac{\sigma \Delta t}{2\varepsilon} + \sum_{j=0}^{\ell} \sum_{i=0}^{\ell} \frac{\alpha_i \beta_j \Delta t \varepsilon_{d_j}}{\varepsilon_\infty (2\tau_i + \Delta t)}$ and $\varepsilon_{d_j} = \varepsilon_{s_j} - \varepsilon_\infty$.

4.3. **Multiple Polarizations.** We now begin to examine the situation in which a material displays multiple polarizations. Since a human tissue sample is made up of different components, within one sample there may be multiple relaxation time and static permittivity parameters. In the example of dry skin, there are two polarization terms, implying two τ_m and two ε_{d_m}. We will use, for the purposes of consistency with the Cole-Cole and Debye models, $\Delta\varepsilon_m$, as opposed to ε_{d_m}, where $\Delta\varepsilon_m = \varepsilon_{s_m} - \varepsilon_{s_{m-1}}$ (except for $\Delta\varepsilon_1$, since $\Delta\varepsilon_1 = \varepsilon_{s_1} - \varepsilon_\infty$). Our total polarization is simply the sum of the polarizations present in the material, so polarization reduces to

$$P(t,z) = P_1 + P_2. \tag{27}$$

Each polarization term is a function of a different relaxation time parameter. We begin by defining P_1 in a similar manner to Equation (20),

$$P_1 = \int_{\tau_1^a}^{\tau_1^b} \mathcal{P}(t,z;\tau) dF_1(\tau), \tag{28}$$

where $\tau_1^a = (1-a_1)\cdot\tau_1$ and $\tau_1^b = (1+b_1)\cdot\tau_1$. The values of a_1 and b_1 are determined by where we want the lower and upper limits of the uniform distribution, τ_1^a and τ_1^b, to be located. P_2 can be similarly defined.

By inputting the density of the uniform distribution, (28) is written as

$$P_1 = \frac{1}{\tau_1^b - \tau_1^a} \int_{\tau_1^a}^{\tau_1^b} \mathcal{P}(t,z;\tau) d\tau, \tag{29}$$

since $dF_1(\tau) = \frac{1}{\tau_1^b - \tau_1^a} d\tau$ for a uniform distribution. Therefore, we can express the material's total polarization as

$$P(t,z) = \frac{1}{\tau_1^b - \tau_1^a} \int_{\tau_1^a}^{\tau_1^b} \mathcal{P}(t,z;\tau) d\tau + \frac{1}{\tau_2^b - \tau_2^a} \int_{\tau_2^a}^{\tau_2^b} \mathcal{P}(t,z;\tau) d\tau. \tag{30}$$

The above considers looking at polarization with distributions for the relaxation time parameters. We now adjust the multiple polarization model to also include distributions for the static permittivity parameters. For the uniform distribution, we have $dG_1(\Delta\varepsilon) = \frac{1}{\Delta\varepsilon_1^d - \Delta\varepsilon_1^c} d\Delta\varepsilon$ and $dG_2(\Delta\varepsilon) = \frac{1}{\Delta\varepsilon_2^d - \Delta\varepsilon_2^c} d\Delta\varepsilon$, where $\Delta\varepsilon_1^c = (1-c_1)\cdot\Delta\varepsilon_1$ and $\Delta\varepsilon_1^d = (1+d_1)\cdot\Delta\varepsilon_1$. The values of c_1 and d_1 are determined by where we want the lower and upper limits of the uniform distribution, $\Delta\varepsilon_1^c$ and $\Delta\varepsilon_1^d$, to be located. Equations (28) and (29) now update to be

$$P_1 = \int_{\Delta\varepsilon_1^c}^{\Delta\varepsilon_1^d} \int_{\tau_1^a}^{\tau_1^b} \mathcal{P}(t,z;\tau,\varepsilon_s) dF_1(\tau) dG_1(\Delta\varepsilon). \tag{31}$$

$$P_1 = \frac{1}{\Delta\varepsilon_1^d - \Delta\varepsilon_1^c} \frac{1}{\tau_1^b - \tau_1^a} \int_{\Delta\varepsilon_1^c}^{\Delta\varepsilon_1^d} \int_{\tau_1^a}^{\tau_1^b} \mathcal{P}(t,z;\tau,\varepsilon_s) d\tau d\Delta\varepsilon. \tag{32}$$

Once again P_2 can be solved similarly. We use these P_1 and P_2 values in (27) to obtain a new polarization term.

Both our electric field and polarization equation must be updated to account for the multiple polarizations. We can start by amending (24) to include both polarization terms

$$\varepsilon\frac{\partial E}{\partial t} = -\frac{\partial H}{\partial z} - \sigma E - \sum_{j=0}^{\ell}\sum_{i=0}^{\ell} \beta_j\alpha_i \frac{\partial \mathcal{P}_{1_{ij}}}{\partial t} - \sum_{j=0}^{\ell}\sum_{i=0}^{\ell} \beta_j\alpha_i \frac{\partial \mathcal{P}_{2_{ij}}}{\partial t}, \tag{33}$$

where $\mathcal{P}_{1_{ij}} = \mathcal{P}(t,z;\tau_{1_i},\Delta\varepsilon_{1_j})$. Using FDTD, we see that

$$\sum_{j=0}^{\ell}\sum_{i=0}^{\ell} \beta_j\alpha_i \frac{\partial \mathcal{P}_{1_{ij}}}{\partial t} \approx \sum_{j=0}^{\ell}\sum_{i=0}^{\ell} \beta_j\alpha_i \frac{[(\mathcal{P}_{1_{ij}})_k^{n+\frac{1}{2}} - (\mathcal{P}_{1_{ij}})_k^{n-\frac{1}{2}}]}{\Delta t}.$$

By combining the summations, Equation (33) updates to be

$$\varepsilon\frac{\partial E}{\partial t} = -\frac{\partial H}{\partial z} - \sigma E - \sum_{j=0}^{\ell}\sum_{i=0}^{\ell}\beta_j\alpha_i\frac{(\mathcal{P}_{1_{ij}})_k^{n+\frac{1}{2}} - (\mathcal{P}_{1_{ij}})_k^{n-\frac{1}{2}} + (\mathcal{P}_{2_{ij}})_k^{n+\frac{1}{2}} - (\mathcal{P}_{2_{ij}})_k^{n-\frac{1}{2}}}{\Delta t}. \tag{34}$$

We also revise (25) to solve for $(\mathcal{P}_{1_{ij}})_k^{n+\frac{1}{2}}$:

$$(\mathcal{P}_{1_{ij}})_k^{n+\frac{1}{2}} = \frac{\Delta t\varepsilon_0\varepsilon_{d1_j}[E_k^{n+\frac{1}{2}} + E_k^{n-\frac{1}{2}}] + (2\tau_{1_i} - \Delta t)(\mathcal{P}_{1_{ij}})_k^{n-\frac{1}{2}}}{2\tau_{1_i} + \Delta t}. \tag{35}$$

We can similarly find an equation for $(\mathcal{P}_{2_{ij}})_k^{n+\frac{1}{2}}$. Using these new expressions for $(\mathcal{P}_{1_{ij}})_k^{n+\frac{1}{2}}$ and $(\mathcal{P}_{2_{ij}})_k^{n+\frac{1}{2}}$, (34) becomes

$$E_k^{n+\frac{1}{2}} = \frac{\theta}{1+\delta}[H_{k+\frac{1}{2}}^n - H_{k-\frac{1}{2}}^n] + \frac{1-\delta}{1+\delta}E_k^{n-\frac{1}{2}} + \sum_{j=0}^{\ell}\sum_{i=0}^{\ell}\frac{2\Delta t\alpha_i\beta_j}{\varepsilon(1+\delta)}\left[\frac{(\mathcal{P}_{1_{ij}})_k^{n-\frac{1}{2}}}{2\tau_{1_i}+\Delta t} + \frac{(\mathcal{P}_{2_{ij}})_k^{n-\frac{1}{2}}}{2\tau_{2_i}+\Delta t}\right], \tag{36}$$

where $\delta = \frac{\sigma\Delta t}{2\varepsilon} + \sum_{j=0}^{\ell}\sum_{i=0}^{\ell}\frac{\alpha_i\beta_j\Delta t}{\varepsilon_\infty}\left(\frac{\varepsilon_{d1_j}}{2\tau_{1_i}+\Delta t} + \frac{\varepsilon_{d2_j}}{2\tau_{2_i}+\Delta t}\right)$ and $\varepsilon_{d1_j} = \varepsilon_{s1_j} - \varepsilon_\infty$.

5. Inverse Problem for Distribution Parameters

5.1. **Motivation for Distributing Dielectric Parameters of Debye Model.** The Cole-Cole model has been considered an excellent way to approximate the true properties of dielectric materials in which multiple mechanisms are present. While uncertain about the true nature of the mechanisms being described by this model, we find that the model is more accurate in comparison to other known models. The data that models such as Cole-Cole attempt to approximate is $\varepsilon(\omega)$, a complex value that reveals measured permittivities and conductivities at different frequencies. In the case of the Cole-Cole model,

$$\varepsilon(\omega)_{CC} = \varepsilon_\infty + \sum_{m=1}^{n}\frac{\Delta\varepsilon_m}{1+(i\omega\tau_m)^{(1-\alpha_m)}} + \frac{\sigma}{i\omega\varepsilon_0}, \tag{37}$$

where each τ_m represents one of the relaxation time parameters, $\Delta\varepsilon_m = \varepsilon_{s_m} - \varepsilon_{s_{m-1}}$ (except for $\Delta\varepsilon_1$, since $\Delta\varepsilon_1 = \varepsilon_{s_1} - \varepsilon_\infty$), and n is the number of poles. We get this $\varepsilon(\omega)$ term by converting Equation (5) to the frequency domain and arriving at

$$\hat{\mathbf{D}} = \varepsilon(\omega)\hat{\mathbf{E}} \tag{38}$$

The FDTD method, as seen earlier, helps to provide researchers with a way of simulating the behavior of electromagnetic fields inside a dielectric. For the Cole-Cole model, however, the FDTD method does not apply because the time domain formulation contains a fractional-order derivative [4]. This eliminates the ease of using FDTD and has encouraged many researchers to use the Cole-Cole model's predecessor, the Debye model, for which the value of $\varepsilon(\omega)$ is computed as

$$\varepsilon(\omega)_D = \varepsilon_\infty + \sum_{m=1}^{n}\frac{\Delta\varepsilon_m}{1+(i\omega\tau_m)} + \frac{\sigma}{i\omega\varepsilon_0}. \tag{39}$$

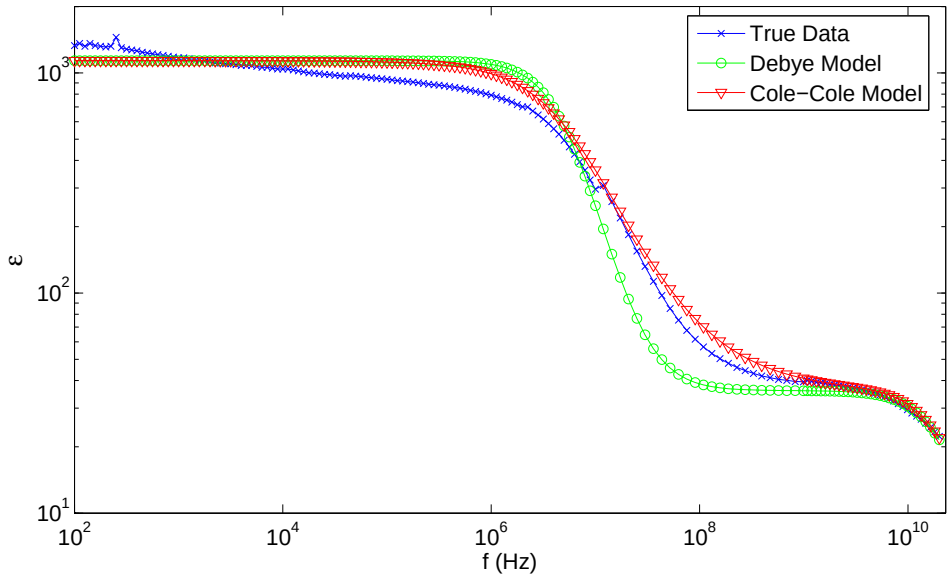

FIGURE 1. Real part of $\varepsilon(\omega)$, ε, or the permittivity.

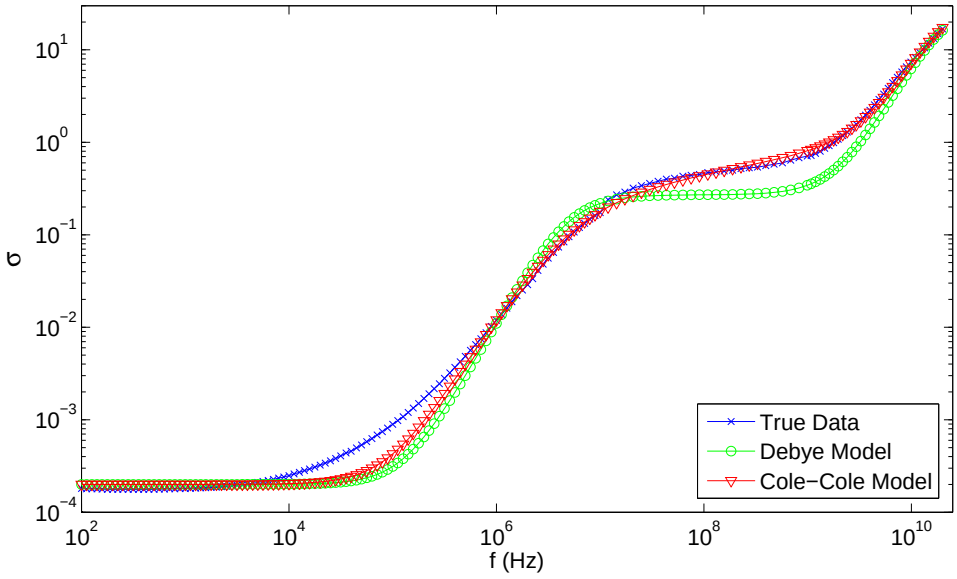

FIGURE 2. Imaginary part of $\varepsilon(\omega)$, σ, or the conductivity.

Figures 1 and 2, which display the complex permittivity and conductivity, show how effective both the Debye model and Cole-Cole model are in approximating the true data for a dry skin tissue sample. It is evident that the Cole-Cole model provides a better fit to the true data than the Debye model. The computational difficulty associated with the Cole-Cole model and the relative ease for the Debye model, however, motivates us to enhance the Debye model in such a way that it better estimates the true data, but is still straight forward to simulate. While the current literature

already suggests [2] that distributed relaxation times make the Debye model a more accurate fit, the question of whether a distribution on the static permittivity parameters improves the model has yet to be considered. We seek to show that with such additional distributions, the Debye model becomes more realistic, as materials actually do display both a range of relaxation times (τ) and a range of static permittivities (ε_s).

5.2. **Inverse Problem Formulation.** Using data for $\varepsilon_\infty, \tau_m$, and ε_{s_m} from Gabriel [6], we were able to produce plots for both the real and imaginary parts of $\varepsilon(\omega)$ for a number of human tissue samples. Each of the τ_m and $\Delta\varepsilon_m$ in the Debye model are given a uniform distribution, using the framework discussed in Section 4. We choose to distribute $\Delta\varepsilon_m$, as opposed to ε_{s_m}, since each of the $\Delta\varepsilon_m$ appear in the actual Cole-Cole and Debye models of $\varepsilon(\omega)$. The distribution of the $\Delta\varepsilon_m$, though, in effect, creates a distribution on each of the static permittivity parameters (excluding ε_∞). Attempting to determine parameters of the distributions, in the case of dry skin where there are two τ_m and two $\Delta\varepsilon_m$ (the case where $n = 2$), results in an eight parameter inverse problem – as each uniform distribution has both a lower and upper limit.

Our Debye model with uniformly distributed dielectric parameters calculates $\varepsilon(\omega)$ differently from the basic Debye model. Performing this calculation requires N Monte Carlo (MC) simulations. For each MC simulation, we randomly sample each τ_{m_k} and $\Delta\varepsilon_{m_k}$, which are distributed as follows

$$\tau_{m_k} \sim \mathcal{U}[(1-a_m)\tau_m, (1+b_m)\tau_m]$$

and

$$\Delta\varepsilon_{m_k} \sim \mathcal{U}[(1-c_m)\Delta\varepsilon_m, (1+d_m)\Delta\varepsilon_m],$$

where a_m, b_m, c_m and d_m are the values of interest in our inverse problem for the distributions of τ_m and $\Delta\varepsilon_m$. Therefore, each MC simulation yields n of both the $\Delta\varepsilon_{m_k}$ and the τ_{m_k} terms, which together produce

$$\varepsilon(\omega)_k = \varepsilon_\infty + \sum_{m=1}^{n} \frac{\Delta\varepsilon_{m_k}}{1+(i\omega\tau_{m_k})} + \frac{\sigma}{i\omega\varepsilon_0}$$

The term $\varepsilon(\omega)$ for the distributed Debye model is simply computed as the sample mean of the $\varepsilon(\omega)_k$,

$$\varepsilon(\omega)_{DD} = \frac{1}{N}\sum_{k=1}^{N} \varepsilon(\omega)_k. \tag{40}$$

We performed two inverse problems: one which looked to retrieve the a_m, b_m, c_m and d_m that fit the Debye model with uniformly distributed dielectric parameters to the true data and another that sought to discover those a_m, b_m, c_m and d_m that would bring the distributed Debye model as close as possible to the Cole-Cole model. To begin the inverse problem we created a cost functional of the relative least squares error form that looked at the difference between both the real and imaginary parts of $\varepsilon(\omega)$. The real part of $\varepsilon(\omega)$ was ε or the permittivity, while the imaginary part was conductivity. We scaled the conductivity as follows

$$\sigma = \Re\left(\varepsilon(\omega) i\omega\varepsilon_0\right).$$

To further simplify calculations, we define $q = [\varepsilon, \sigma]$. Our cost functional was simply

$$J = \sum_{i=1}^{n} \left(\frac{q_{DD_i} - q_i}{q_i}\right)^2 = R^{\mathrm{T}}R, \tag{41}$$

where q_{DD} represents the vector for the distributed Debye model, q is the vector for the true data and $R_i = \frac{q_{DD_i} - q_i}{q_i}$. For the inverse problem that attempted to approximate the Cole-Cole model, the cost functional is instead

$$J = \sum_{i=1}^{n} \left(\frac{q_{DD_i} - q_{CC_i}}{q_{CC_i}} \right)^2, \tag{42}$$

where q_{CC} represents the vector for the Cole-Cole model.

Before beginning the optimization routine to minimize the cost functional, we must select an appropriate number, N, of MC simulations to compute $\varepsilon(\omega)_{DD}$. To do this, we choose N such that the variability of the $\varepsilon(\omega)$ term begins to converge to zero. Figure 3 displays the variability

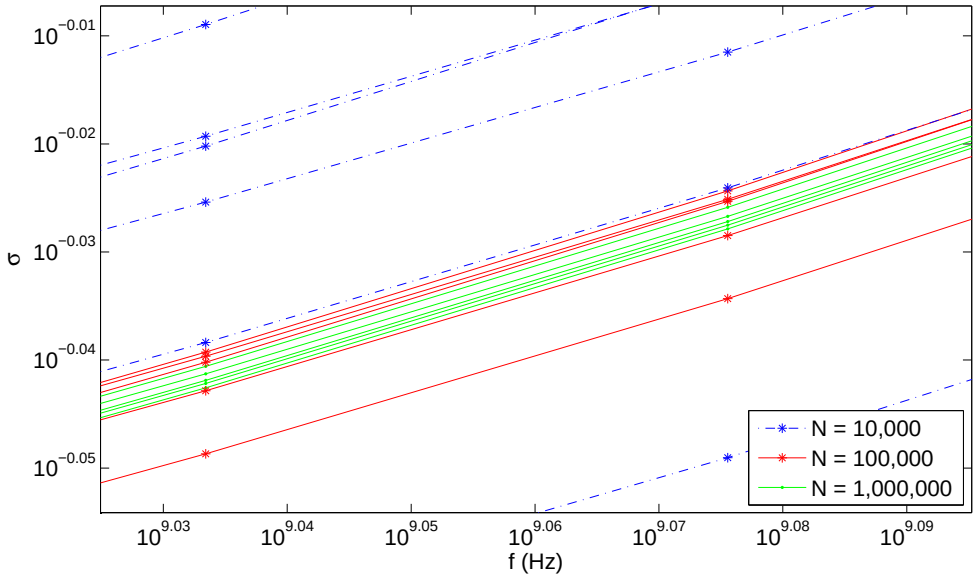

FIGURE 3. This figure shows five random plots of conductivity for each of N = 10,000, 100,000, and 1,000,000 at a very high resolution.

of σ for a varying number of MC simulations. At this resolution, the figure suggests that the variability of σ converges to zero as N increases. By the Kramer-Kronig relationship [7], we can infer that the same holds true for permittivity and therefore the entire $\varepsilon(\omega)$ term. For this reason, we believe $N = 1,000,000$ to be a sufficient number of MC simulations for our inverse problem, while recognizing that increasing N further could produce more exact results.

5.3. **Distributed Debye Fit to Cole-Cole Model.** Before performing the eight parameter inverse problem for the Cole-Cole model, we attempted to solve the four parameter inverse problem, which only placed distributions on the τ_m (from here on referred to as Model A). Our first step in minimizing the cost functional was to search for the region in which a global minimum occurs. We recognized that we could place some constraints on our optimization problem that we believed to be reasonable for an inverse problem of this nature. We restricted the a_m values to be less than or equal to one, so that we would never sample a value of the relaxation time, τ_m, that was less than zero. These values were also restricted to be greater than or equal to zero, so that sampling does not occur only at values that are strictly larger than those of Gabriel's Cole-Cole τ values i.e. the

values found in [6] are inside the intervals defining the distributions. Based on observations, we noticed that both τ_1 and τ_2 tended towards distributions where the mean was slightly greater than the data's parameter values. This encouraged us to allow both b_1 and b_2 to be less than or equal to two. The set of constraints on the problem was

$$\begin{array}{ll} a_1 \in [0,1] & b_1 \in [0,2] \\ a_2 \in [0,1] & b_2 \in [0,2]. \end{array} \tag{43}$$

We ran Finkel's Direct program [5], a MATLAB code which performs constrained optimization in order to approximate the global minimum subject to the constraints mentioned above. The algorithm [8] works by determining a region that may contain the solution, then the program continuously refines this region until it exceeds the allowable number of function evaluations. The only value that Direct retrieved that pushed against the bounds of the constraints was a_2, which stayed quite close to one. Figure 4 indicates that the optimal value of a_2 to achieve a minimal cost is one. In Appendix A is the entire set of plots that display how sensitive cost is when varying distribution parameters. Since none of the other values that Direct found were pushing against the bounds of the constraints set in the program, we were satisfied that these were reasonable constraints.

The Direct program's retrieved values and the corresponding cost of the distributed Debye model with these distribution parameters versus the Cole-Cole model were

$$\begin{array}{ll} a_1 = 0.5554 & b_1 = 1.3347 \\ a_2 = 0.9980 & b_2 = 1.3329 \end{array}$$

$$J = 1.7910.$$

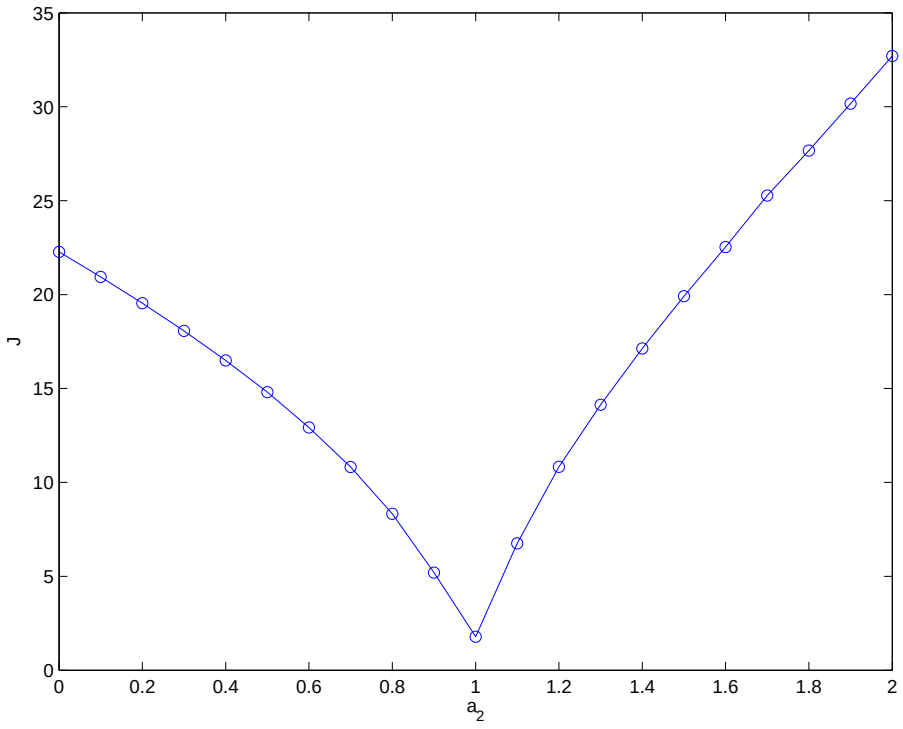

FIGURE 4. The relative cost, with all other distribution parameters constant, as a_2 varies.

We proceeded to perform the same optimization problem with distributions on both relaxation time and static permittivity parameters (from here on referred to as Model B). The constraints for c_m values were reasoned in a similar fashion to the a_m values. Observations did not point to any special constraints for d_m. Since we believe Gabriel's values to be fairly reasonable for each $\Delta\varepsilon_m$ and did not want to go more than 100% on either side, we restricted the d_m values to be less than one as well. The updated constraint set is

$$\begin{array}{ll} a_1 \in [0,1] & b_1 \in [0,2] \\ a_2 \in [0,1] & b_2 \in [0,2] \\ c_1 \in [0,1] & d_1 \in [0,1] \\ c_2 \in [0,1] & d_2 \in [0,1]. \end{array} \tag{44}$$

After running the Direct program, we found the solution to the eight parameter inverse problem matching to Cole-Cole and the corresponding cost to be

$$\begin{array}{ll} a_1 = 0.8882 & b_1 = 1.5569 \\ a_2 = 0.9938 & b_2 = 1.3329 \\ c_1 = 0.5544 & d_1 = 0.8169 \\ c_2 = 0.5123 & d_2 = 0.4922 \end{array}$$

$$J = 1.4651.$$

Figures 5 and 6 show how well both Model A and Model B match up to the actual Cole-Cole model. While it is clear from Figures 5 and 6 that both models match up well with Cole-Cole, it remains to be shown that adding distributions to the static permittivity parameters is an improvement over Model A. To do this, we plot the relative costs, in comparison to the Cole-Cole model, in Figure 7. We believe that Model B presents a much better fit to Cole-Cole primarily because of its low costs at high frequencies.

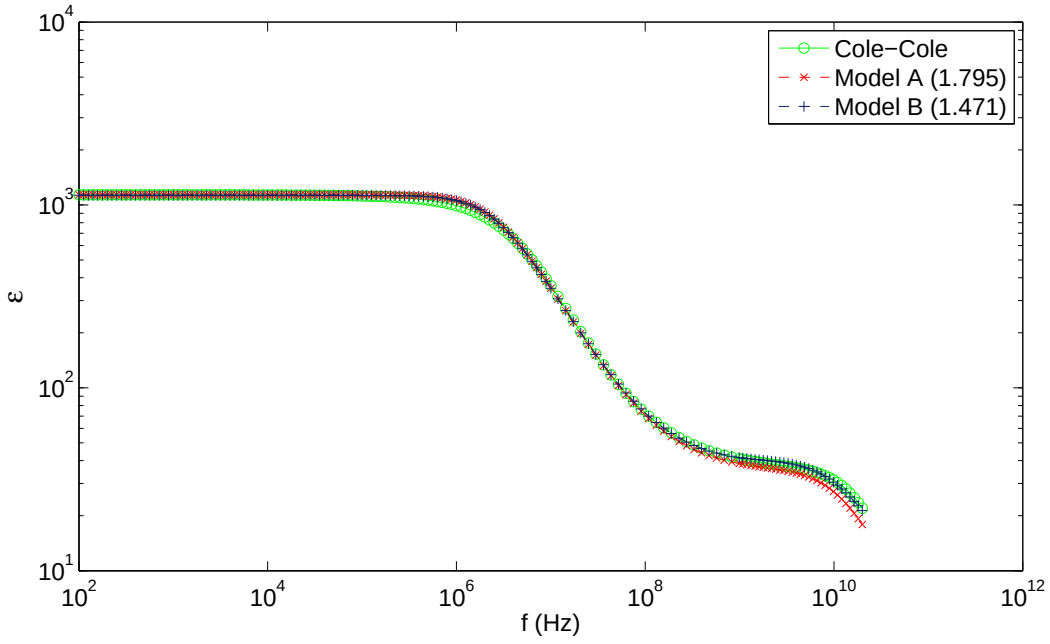

FIGURE 5. Real part of $\varepsilon(\omega)$, ε, or the permittivity.

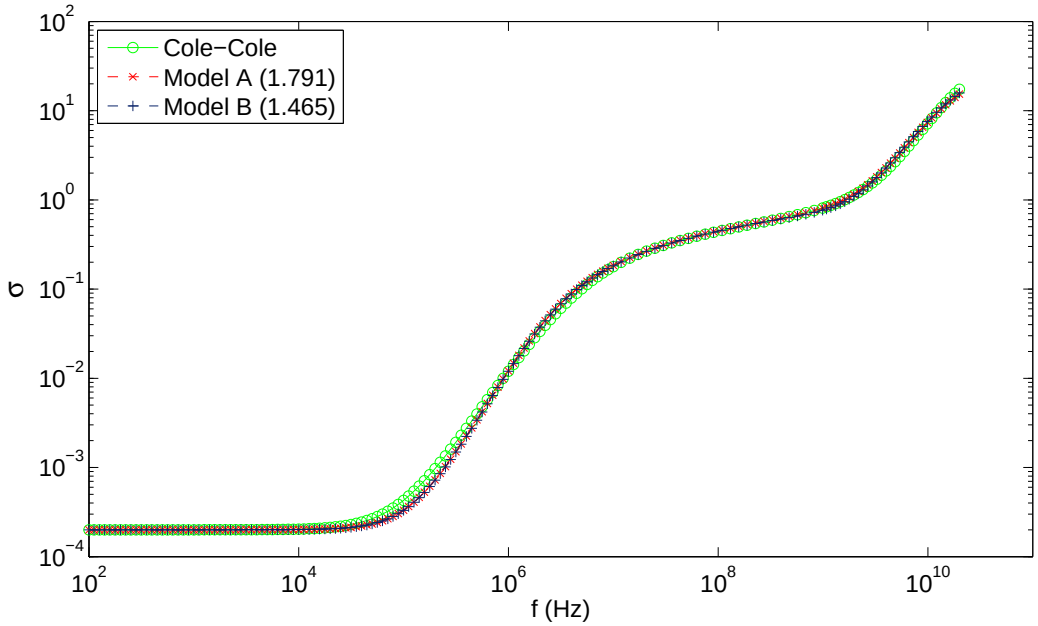

FIGURE 6. Imaginary part of $\varepsilon(\omega)$, σ, or the conductivity.

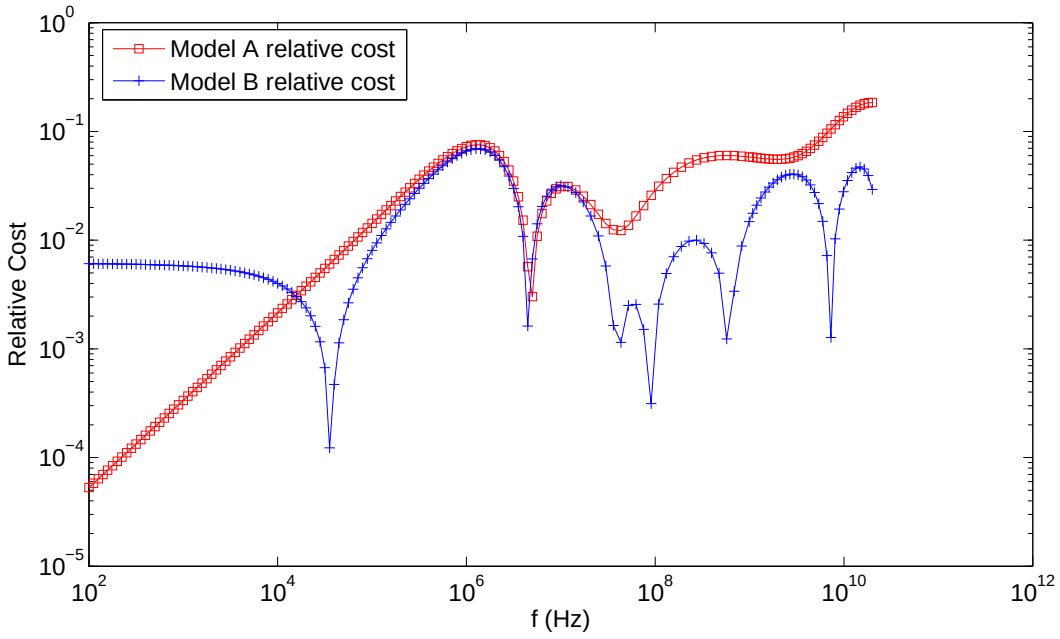

FIGURE 7. The relative costs between Model A and the Cole-Cole model and between Model B and the Cole-Cole model.

It is worth mentioning, however, that while it appears that Model B is definitely a better match to Cole-Cole than Model A, the static permittivity parameters used in Model A were discrete estimates supplied by [6]. We did not perform an optimization routine to search for a minimum cost with distributions of relaxation times along with permittivity parameters varying at different discrete values. Further research could be done to discover if the permittivity parameters truly should be distributed or if they should be discrete but at values other than the ones provided by [6].

5.4. **Distributed Debye Fit to True Data.** In this section, we attempt to determine distribution parameters for the dry skin Debye model that make the model a closer fit to the true data. As a basis of comparison, we will use both the Debye and Cole-Cole models. Using Equation (41), the cost for the Debye model (substituting q_D for q_{DD}) is $J_D = 27.7908$, while the cost for the Cole-Cole (substituting q_{CC} for q_{DD}) is $J_{CC} = 10.4027$. We once again begin by looking at the four parameter inverse problem in which distributions are included only for relaxation time parameters (from here on referred to as Model C). We use the same constraints as in (43). The solution garnered by Direct and the corresponding cost are

$$\begin{array}{ll} a_1 = 0.5508 & b_1 = 1.5569 \\ a_2 = 0.9938 & b_2 = 1.5542 \end{array} \tag{45}$$

$$J = 13.6037.$$

As has been documented [2, 3], distributing the relaxation time parameters presents a significant improvement in cost on the basic Debye model, while still falling short of the Cole-Cole model in approximating the true data. We proceed to extend this to the eight parameter inverse problem with distributions on both the relaxation time and static permittivity parameters (from here on referred to as Model D1). Using the same constraints as in (44), the results and cost are

$$\begin{array}{ll} a_1 = 0.6522 & b_1 = 1.5844 \\ a_2 = 0.9870 & b_2 = 1.3320 \\ c_1 = 0.6522 & d_1 = 0.8402 \\ c_2 = 0.6358 & d_2 = 0.4620 \end{array} \tag{46}$$

$$J = 12.7981.$$

The lower cost signifies a marked upgrade on Model C. Observing the output of the Direct program clued us in to the general trends of the distribution parameters. While the output often stated that a_2 was marginally less than one, we believed that by starting the optimization routine at one, a_2 would stay at one and give us a lower cost. The other side of the τ_2 distribution seemed to be seeking a higher value. Figure 8 displays that higher values of b_2 are related with lower costs. For a full set of figures showing how cost was affected by varying distribution parameter values, refer to Appendix B. We wanted to make sure that all constraints had unit length, so other constraints were adjusted accordingly. The update of the constraint set (for what we refer to as Model D2) from (44) is

$$\begin{array}{ll} a_1 \in [0,1] & b_1 \in [0,1] \\ a_2 \in [.5,1.5] & b_2 \in [1,2] \\ c_1 \in [0,1] & d_1 \in [0,1] \\ c_2 \in [0,1] & d_2 \in [0,1]. \end{array} \tag{47}$$

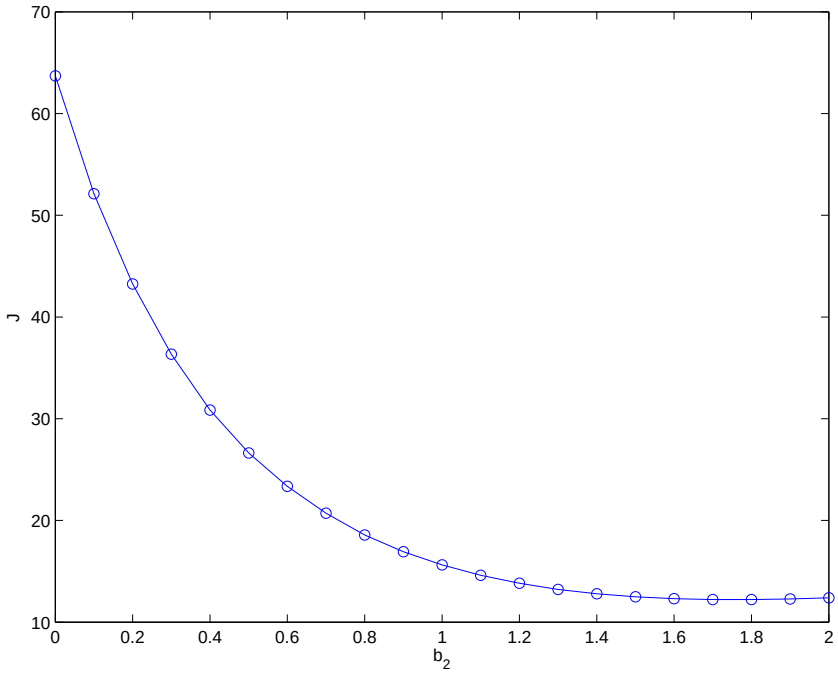

FIGURE 8. The relative cost, with all other distribution parameters constant, as b_2 varies.

We ran Direct to see if this updated set of constraints had any effect on the cost. The results were

$$\begin{aligned} a_1 &= 0.1337 \quad b_1 = 0.6646 \\ a_2 &= 1.0000 \quad b_2 = 1.7840 \\ c_1 &= 0.4630 \quad d_1 = 0.5000 \\ c_2 &= 0.5988 \quad d_2 = 0.4630 \end{aligned} \tag{48}$$

$$J = 12.1945.$$

The uniform distributions that correspond with our output values can be found in Figures 9 and 10.

While our intuition was correct, the cost did become lower, there remained questions about the new output values because each function evaluation is after all a random process. Producing 50 random costs between Model D1 and the true data, we found there to be a variance of 9.6242×10^{-6}. Producing another 50 random costs using the values from Model D2, we found there to be a variance of 9.5164×10^{-5}. This variance is small enough to conclude that this model is, with near certainty, a lower cost model than D1. Also note that the values of the solution parameters in (46) and (48) are significantly different. This underscores the difficulty of minimizing such a cost functional and is part of the reason that gradient-based methods fail.

Figures 11 and 12 show how well Model C, Model D1, and Model D2 match up to the true data. While it is clear from Figures 11 and 12 that all three models fit closely to the data, it needs to be shown that adding distributions to the static permmittivity parameters is an improvement over the model which only distributes relaxation times. To do this, we plot the relative costs, in comparison to true data, in Figure 13. It is apparent that at the higher frequencies, Model D2 has a significantly lower cost than Model C. We believe that the extra distributions on static permittivity parameters are causing this better fit.

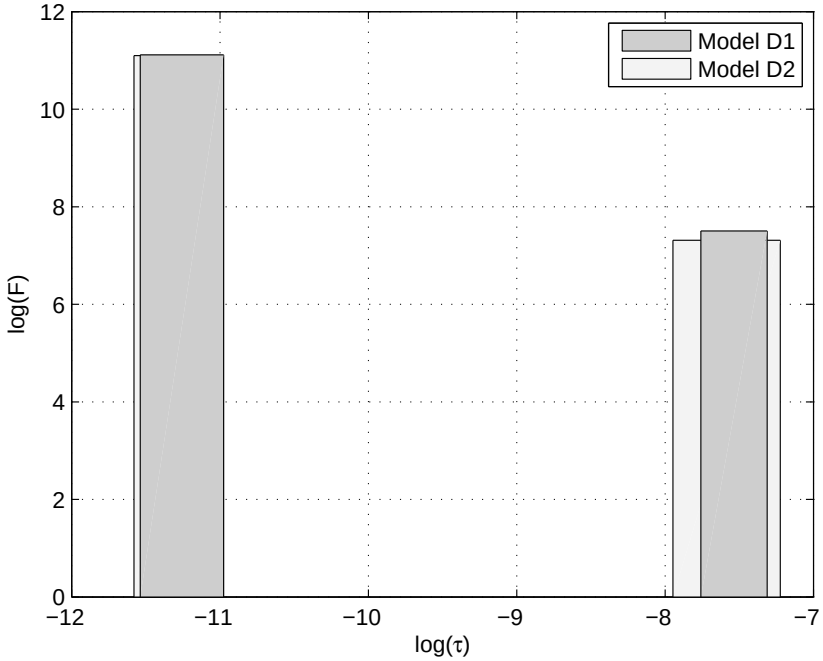

FIGURE 9. Uniform distributions for τ_1 and τ_2 values.

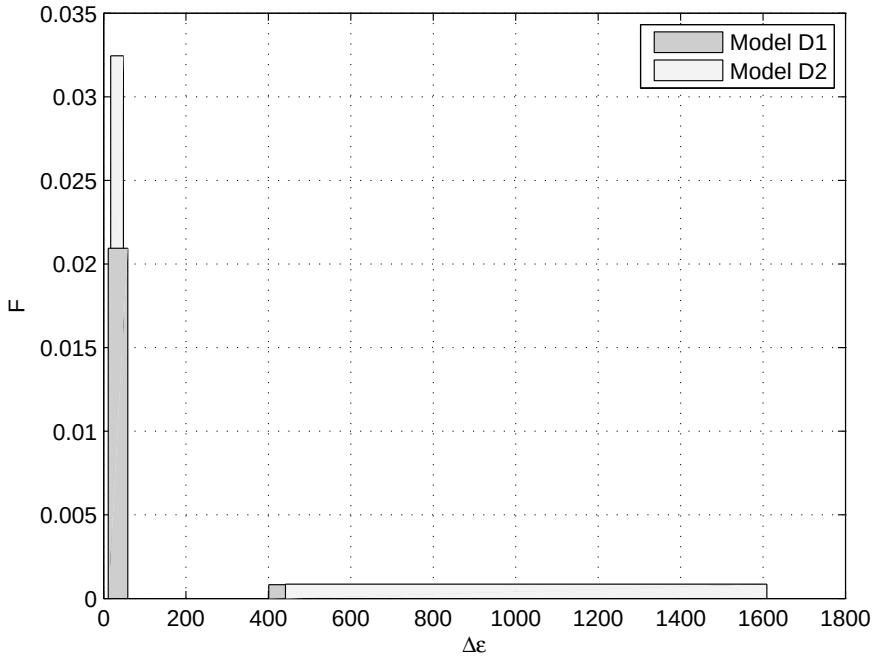

FIGURE 10. Uniform distributions for $\Delta\varepsilon_1$ and $\Delta\varepsilon_2$ values.

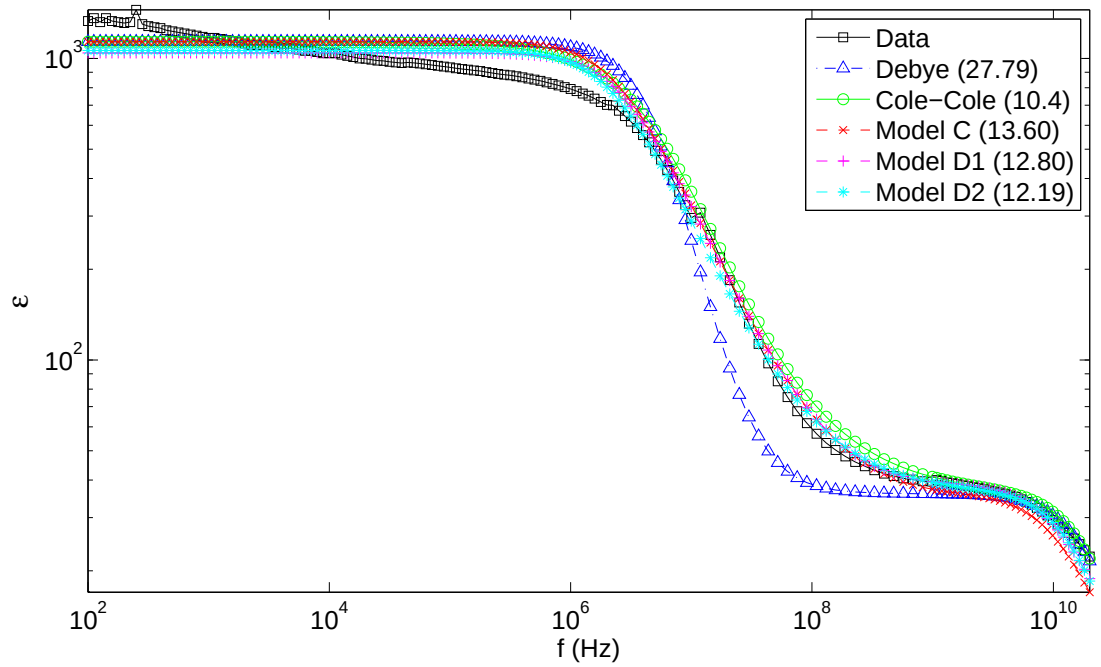

FIGURE 11. Real part of $\varepsilon(\omega)$, σ, or the permittivity.

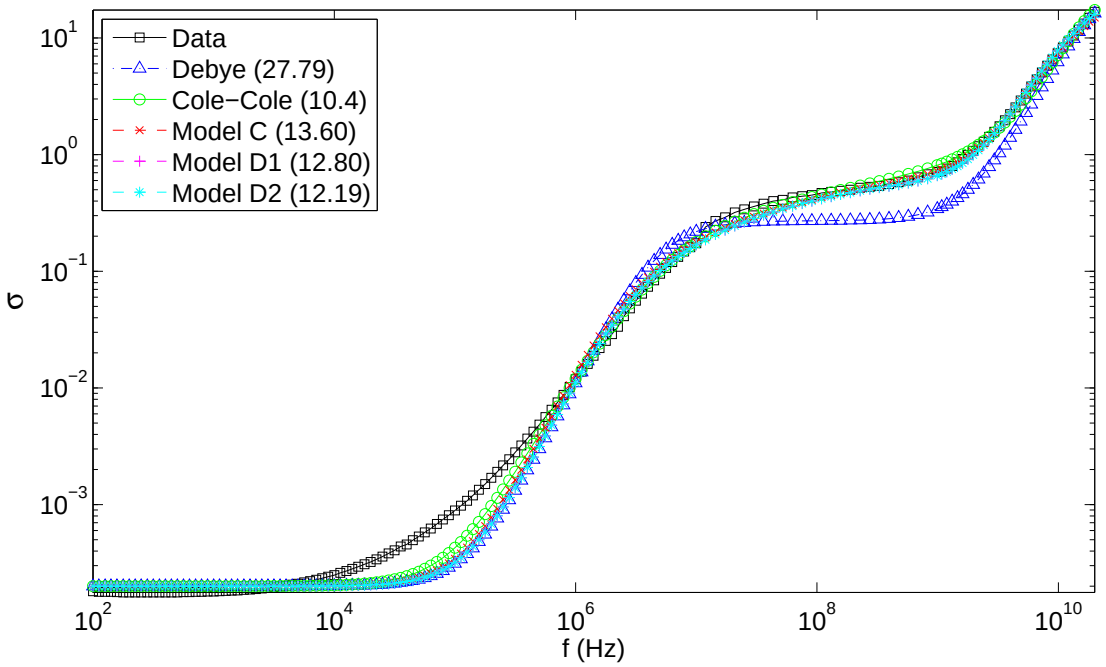

FIGURE 12. Imaginary part of $\varepsilon(\omega)$, σ, or the conductivity.

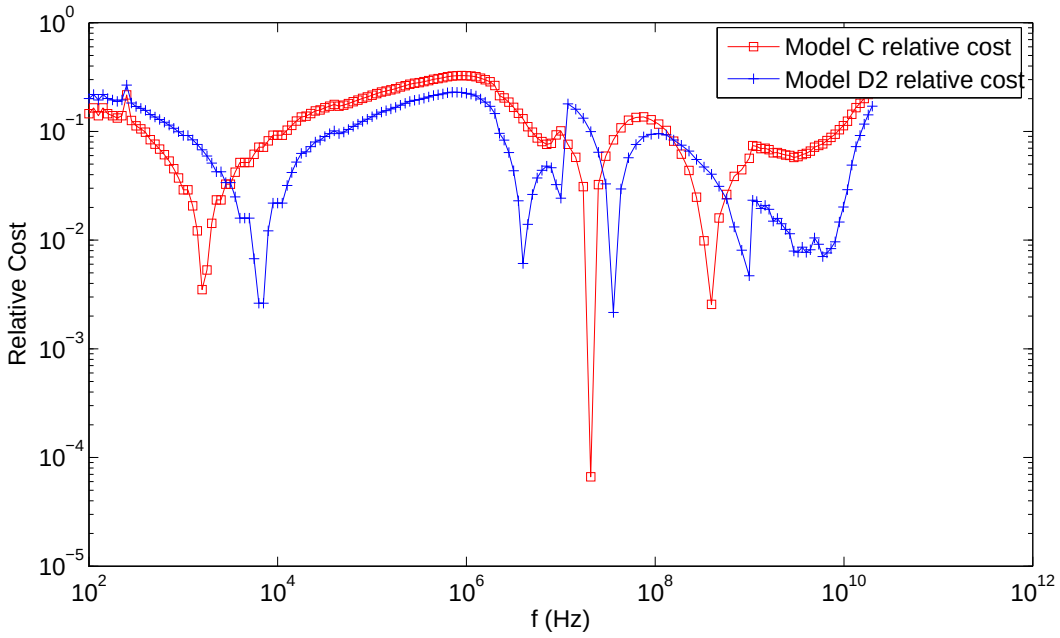

FIGURE 13. The relative costs between Model C and the true data and between Model D2 and the true data.

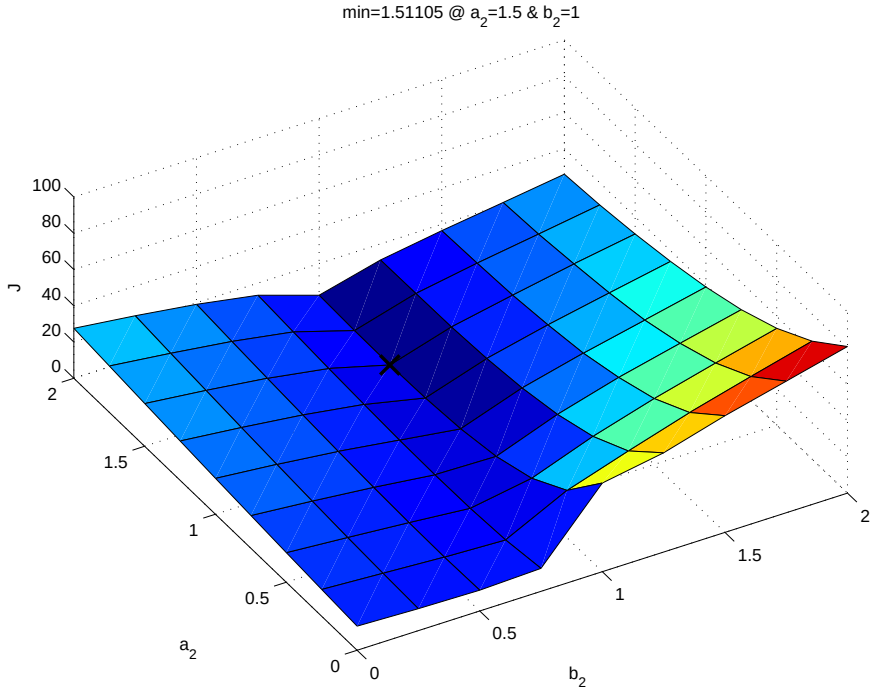

FIGURE 14. The relative cost, with all other distribution parameters constant, as a_2 and b_2 vary.

As a note, much time was devoted to the search for a local minimum in the area of the solutions retrieved by Direct. A code implementing the Gauss-Newton Algorithm was developed and geared towards solving this specific inverse problem. In addition, MATLAB programs such as `fminsearch` and `fmincon` (`fminsearch` subject to a set of constraints) were also used. In each attempt the algorithms failed to traverse a descent direction. Mentioned in [6] is the difficulty of using classical numerical least-squares minimization techniques. The randomness of the inverse problem will often send the algorithm in the wrong direction. Figure 14 shows that in the presence of a "trench", gradient-based approaches can be unreliable. Methods for determining the minimum of stochastic cost functionals is another area which can be explored further.

6. Forward Simulation

6.1. **Setup of Simulator.** In practice, known dielectric parameters of a material are used in computational methods to simulate sending a pulse into a dielectric. To display the practicality of the distributed Debye model, we must show that it is possible to run simulations with uniformly distributed dielectric parameters. Using the FDTD equations described in Section 4, we created a code comparable to that used by Banks et al [1]. Since our code used the updated FDTD equations, however, it also allowed for distributions on the dielectric parameters. We seek to reproduce Figures 4.2 and 4.4 in [1], which display simulations of a truncated sine wave at $t = 5.0$ ns and $t = 10.0$ ns, respectively, through a dielectric material with parameter values

$$\sigma = 1.0 \times 10^{-2} \text{Ohm}^{-1}$$

$$\tau = 1.0 \times 10^{-11} \text{ seconds}$$

$$\varepsilon_s = 35 \text{ relative static permittivity}$$

$$\varepsilon_\infty = 5.$$

By setting the a_m, b_m, c_m and d_m values equal to zero in our code, we no longer had distributions on the dielectric parameters. The lack of distributions on the parameters leaves Figure 15 as comparable to the figures in [1].

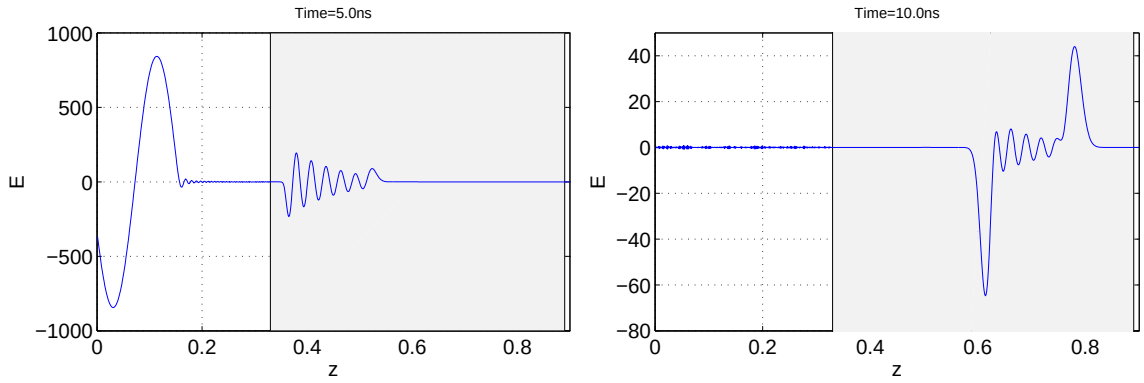

FIGURE 15. Debye model simulations, as done in Figures 4.2 and 4.4 in [1], for ($t = 5.0$ ns) and ($t = 10.0$ ns).

The pulse used in [1] was a truncated sine pulse. We, however, wish to use a UWB pulse to fully excite all poles in the polarization model since the dielectric parameters vary over a broad range of

frequencies. We define our UWB pulse as

$$\sum_{i=1}^{n} \alpha_i sin(2\pi f_i(t)), \tag{49}$$

where f_i is linearly spaced from zero to 1×10^{10} and α_i is defined by the beta distribution, $\beta(2,5)$. After adding this to our code, we needed to ensure that this addition was done correctly. First, we wanted to make sure that the pulse sent through the dielectric attenuated properly in comparison to the pulse sent through free space. We also plotted the Fast Fourier Transform (FFT) of the signal through both free space and the dielectric to ensure that the breadth of the FFT plot for the dielectric was smaller than that of the FFT plot for free space. Figure 16 confirms that the UWB pulse acts in accordance with these properties.

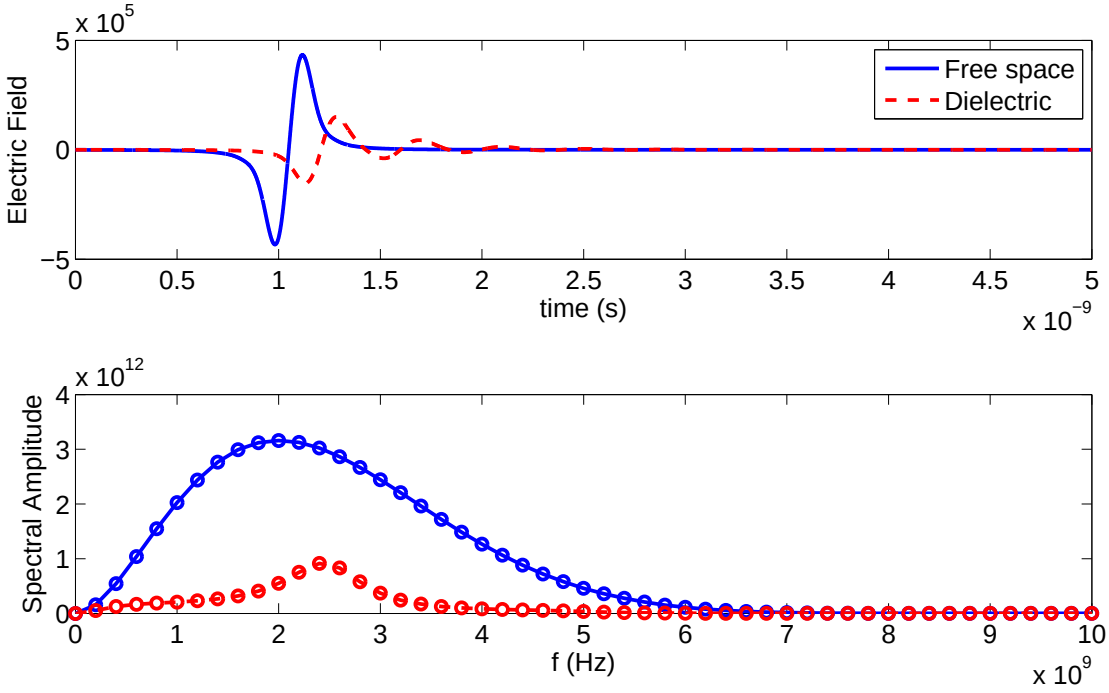

FIGURE 16. The top plot shows the value of the electric field at x=0.0155 as time varies. The dielectric begins at x=0.005 and ends at x=0.015. The bottom plot shows the FFT of the two signals.

6.2. **Forward Simulations.** The applications of forward simulations in computational electromagnetics are abundant and varied. The ability to observe a pulse moving through a dielectric allows us to learn more about both the dielectric properties and geometry of the material in question [1]. Possibly of more significance, however, is the role that forward simulations play in inverse problems which seek to reconstruct the values of dielectric parameters. The forward simulation provides us with a prediction and the object is to "minimize a suitable measure of the difference between the simulated prediction and a set of data taken from experiments"[1]. The benefits of retrieving such parameter values are wide-ranging and well documented [1]. Therefore, for the

distributed Debye model to hold much relevance in the field and for it to be used in a constructive way, it must be applicable to forward simulations.

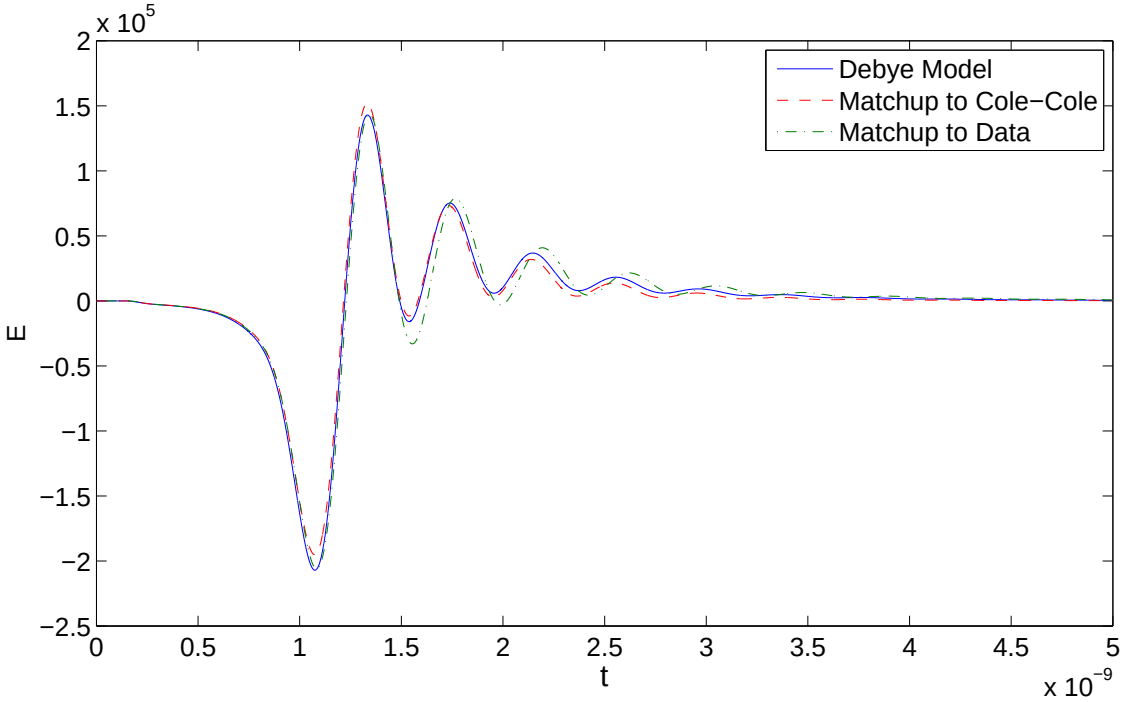

FIGURE 17. Time plot of Electric Field with receiver at x=0.0155. The Debye model with no distributions is plotted against the Debye model with distribution parameters that match up to Cole-Cole and the Debye model with distribution parameters that match up to the true data.

Our choice of dielectric material, for the purpose of example, remains the dry skin tissue investigated in the inverse problem in Section 5. Using dielectric parameter data from [6], we began by running simulations of the Debye model with no distributions on the parameters. We proceeded to run further simulations, distributing the parameters in accordance with the results of our inverse problems. Proper simulations of the distributed Debye model would show that the time trace of the electric field at the receiver was changed only a reasonable amount. Figure 17 shows a simulation of the Debye model with no distribution on dielectric parameters, with distribution parameters found in Model B and with distribution parameters found in Model D2. The fact that the distributed Debye models show some movement away from the Debye model is a positive sign. We, however, cannot be sure how realistic this simulation is until proper interrogation experiments are done with human dry skin tissue samples.

7. CONCLUSION

The Debye model with uniformly distributed relaxation time parameters provides a much closer fit to the Cole-Cole model or the true data than the basic Debye model. Both plots and cost functional outputs suggest that additionally distributing static permittivity parameters is a significant addition to the distributed Debye model, making it a much better approximation than any other Debye model. Although as previously mentioned, using discrete values different from those found

in [6] may produce a different outcome. We have shown that it is straight-forward to implement an FDTD method for the forward solution of our Debye model with distributions, as opposed to the Cole-Cole model. Simulations of the Debye model with uniformly distributed dielectric parameters display a noticeable difference in the behavior of the dielectric material, in comparison to the basic Debye model, that we believe make the simulations more realistic – this, however, cannot be verified without an actual interrogation experiment. There remain many other unanswered questions about this new model and open areas for future research.

The variance of our cost was of the order of 10^{-5} when using $N = 1,000,000$ Monte Carlo simulations. In optimization routines, it is possible that an arbitrary set of distribution parameters will give an abnormally low cost by chance. With access to greater computing speeds, we can run more Monte Carlo simulations and be more confident that the answers we receive are stable and producing more consistent costs.

A possibility for future research is including a pole to the low frequency section of data. Figures 11 and 12 display how poorly all of these models fit to the true data at lower frequencies. We believe that by adding another pole to the data in [6], these models can do a more effective job of approximating the true values. Local minimization and gradient based methods for stochastic problems is another area that needs to be improved upon.

Lastly, the distributed Debye model never provides a closer approximation to the true data than the Cole-Cole model. Our cost outputs always displayed costs greater than 10.4027, the cost between the Cole-Cole model and true data. This implies that there remains room for improvement in approximating the true data. An area for future research is applying distributions other than the uniform distribution to multiple dielectric parameters. We believe that distributions such as the normal or log-normal could provide interesting insight into how a Debye model with distributed dielectric parameters can better approximate true data.

8. APPENDIX A

Appendix A uses the data retrieved in the eight parameter fit to the Cole-Cole model. Each figure shows how the relative cost is affected by varying distribution parameters.

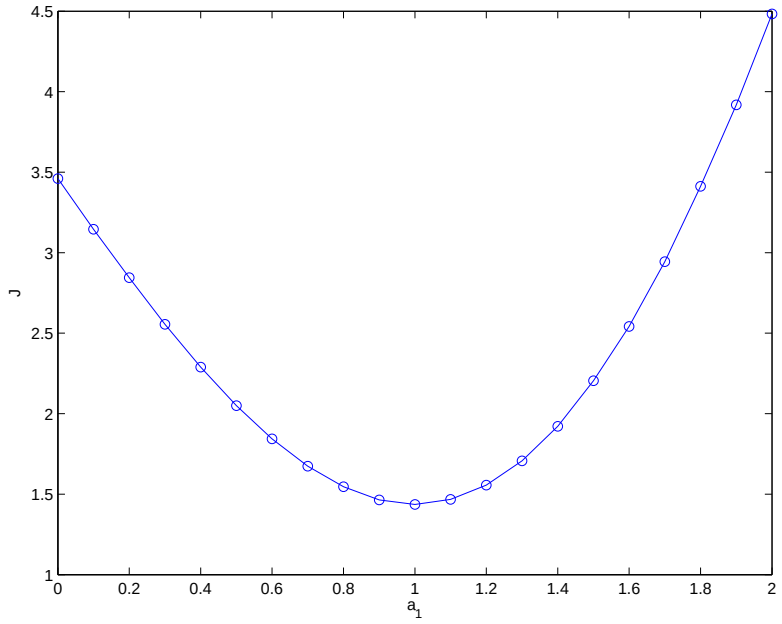

FIGURE 18. The relative cost, with all other distribution parameters constant, as a_1 varies.

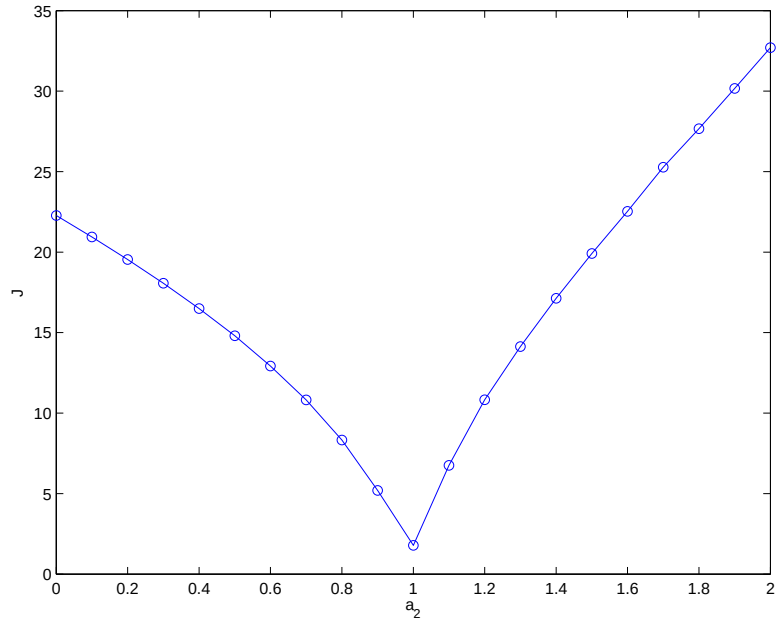

FIGURE 19. The relative cost, with all other distribution parameters constant, as a_2 varies.

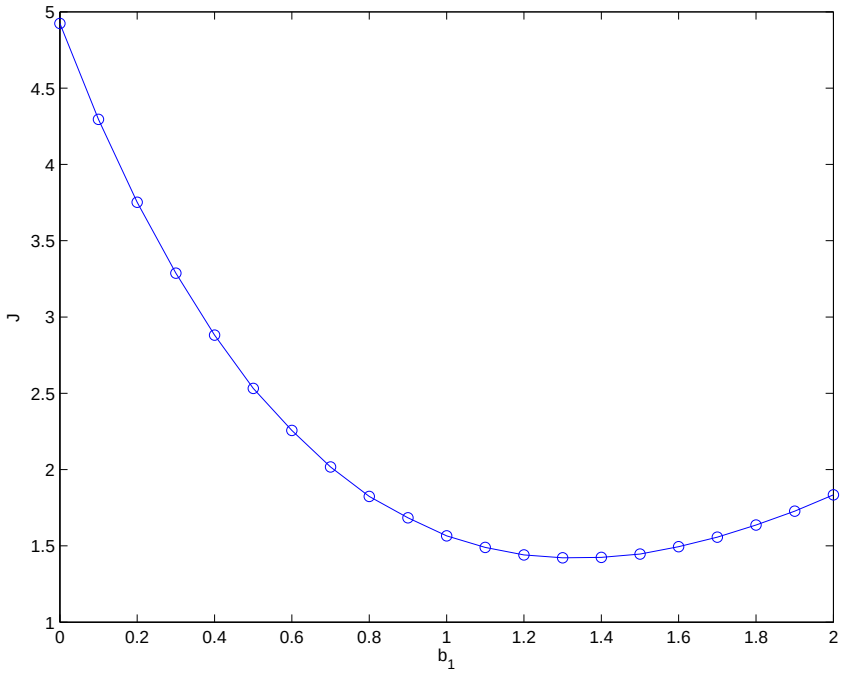

FIGURE 20. The relative cost, with all other distribution parameters constant, as b_1 varies.

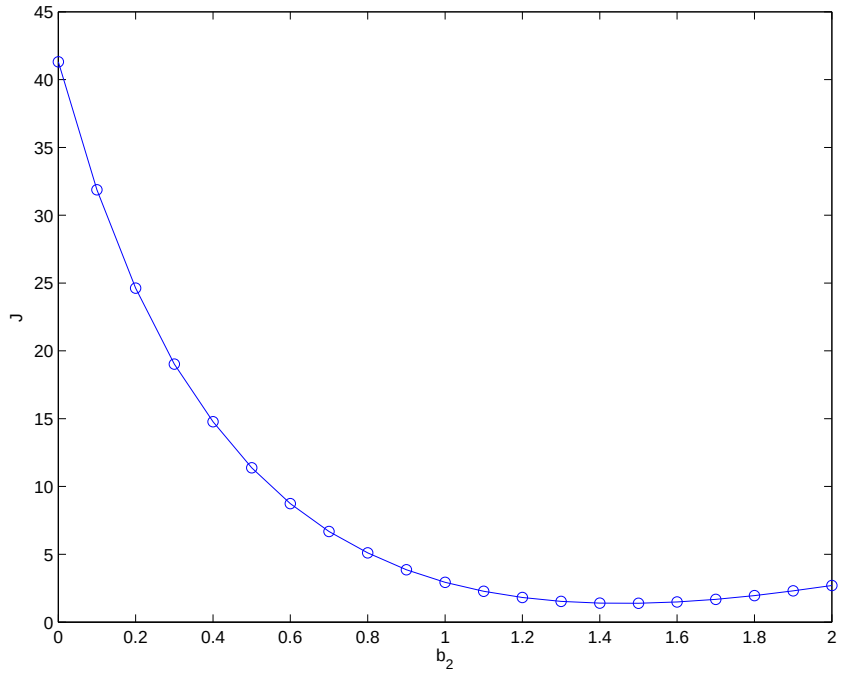

FIGURE 21. The relative cost, with all other distribution parameters constant, as b_2 varies.

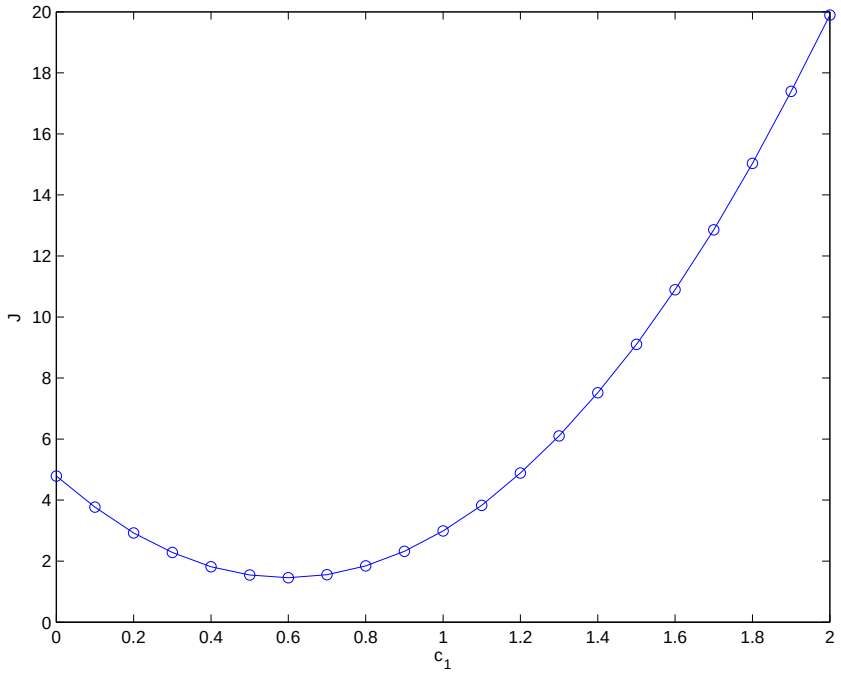

FIGURE 22. The relative cost, with all other distribution parameters constant, as c_1 varies.

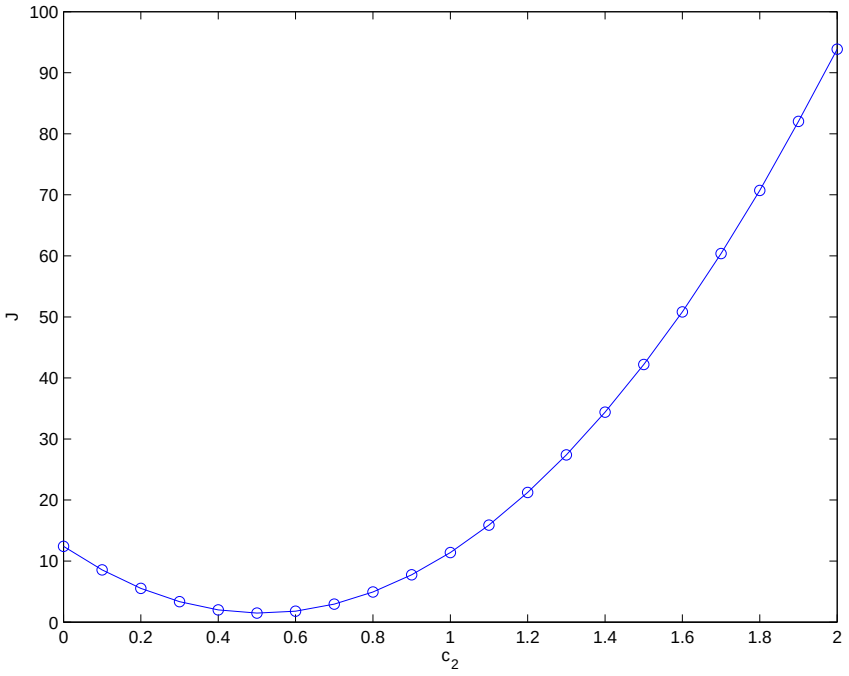

FIGURE 23. The relative cost, with all other distribution parameters constant, as c_2 varies.

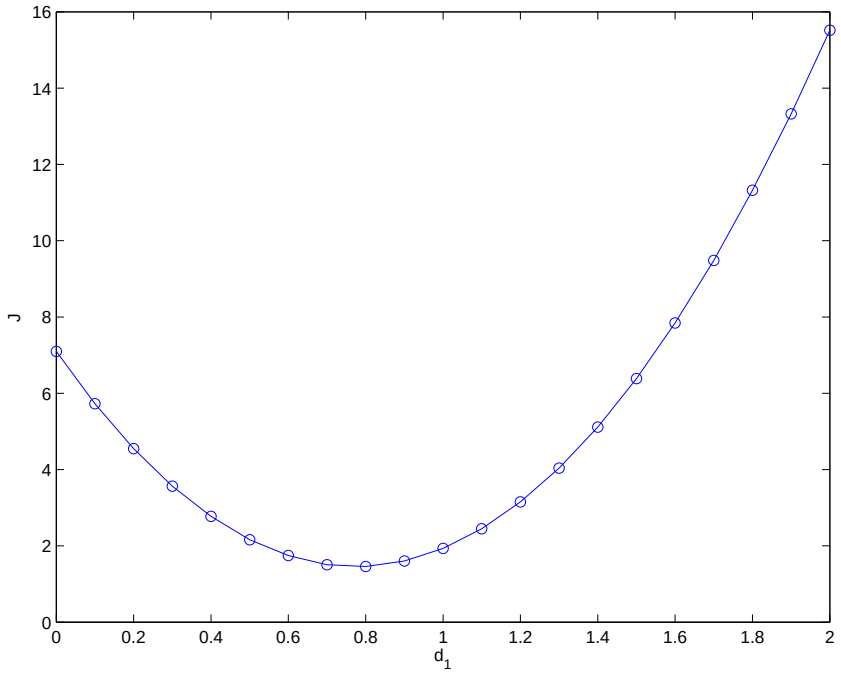

FIGURE 24. The relative cost, with all other distribution parameters constant, as d_1 varies.

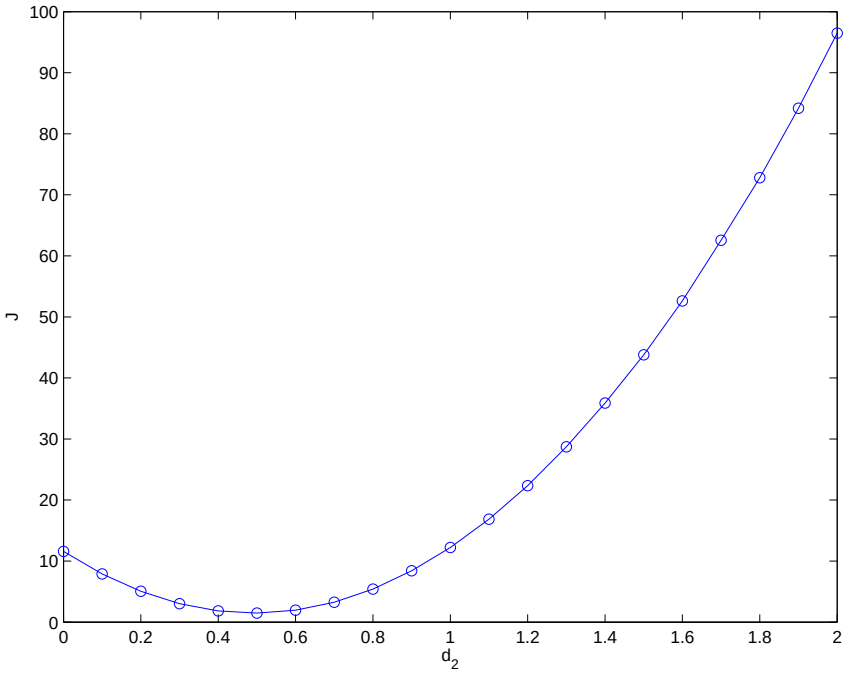

FIGURE 25. The relative cost, with all other distribution parameters constant, as d_2 varies.

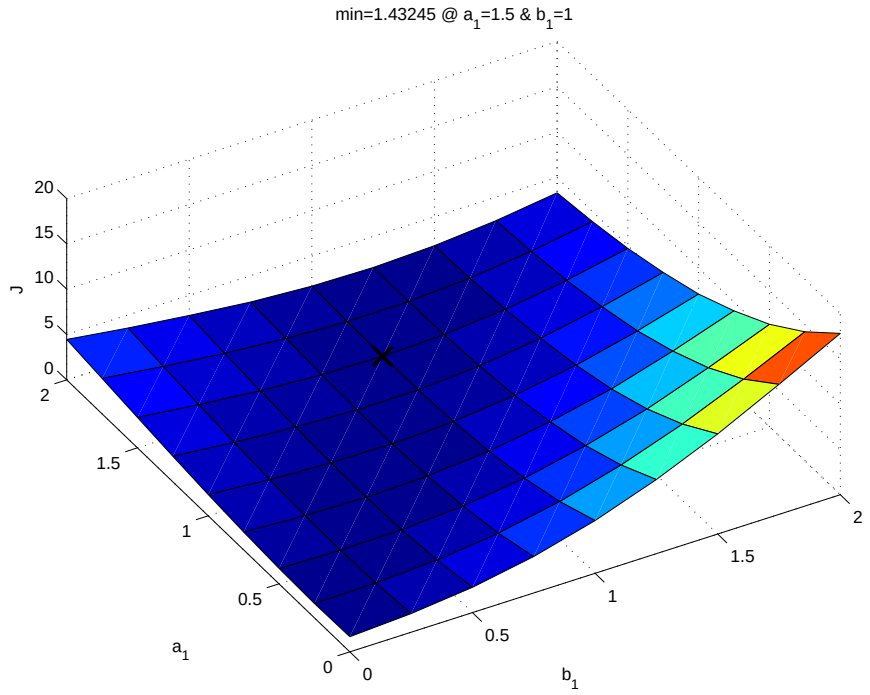

FIGURE 26. The relative cost, with all other distribution parameters constant, as a_1 and b_1 vary.

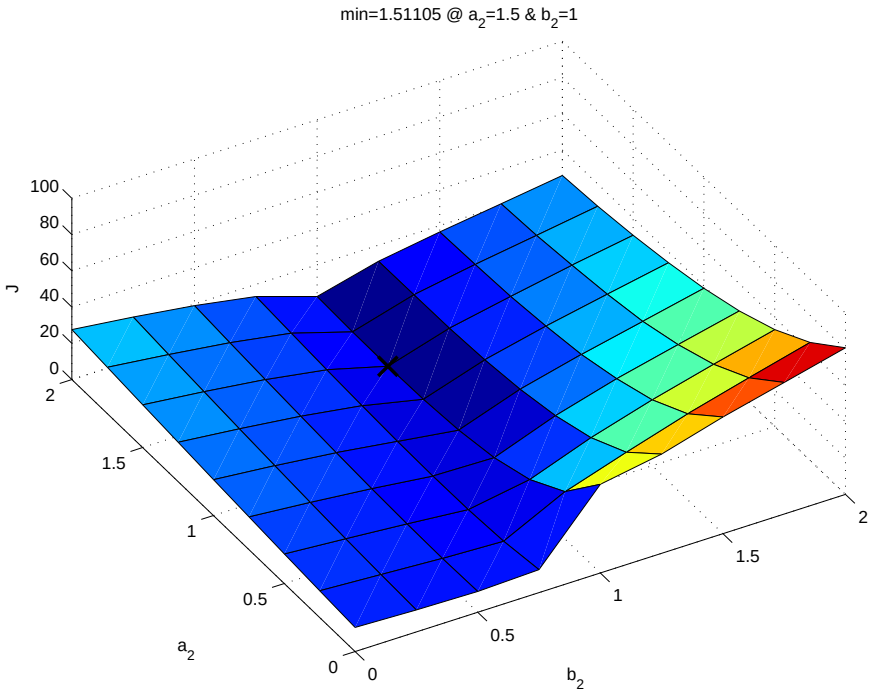

FIGURE 27. The relative cost, with all other distribution parameters constant, as a_2 and b_2 vary.

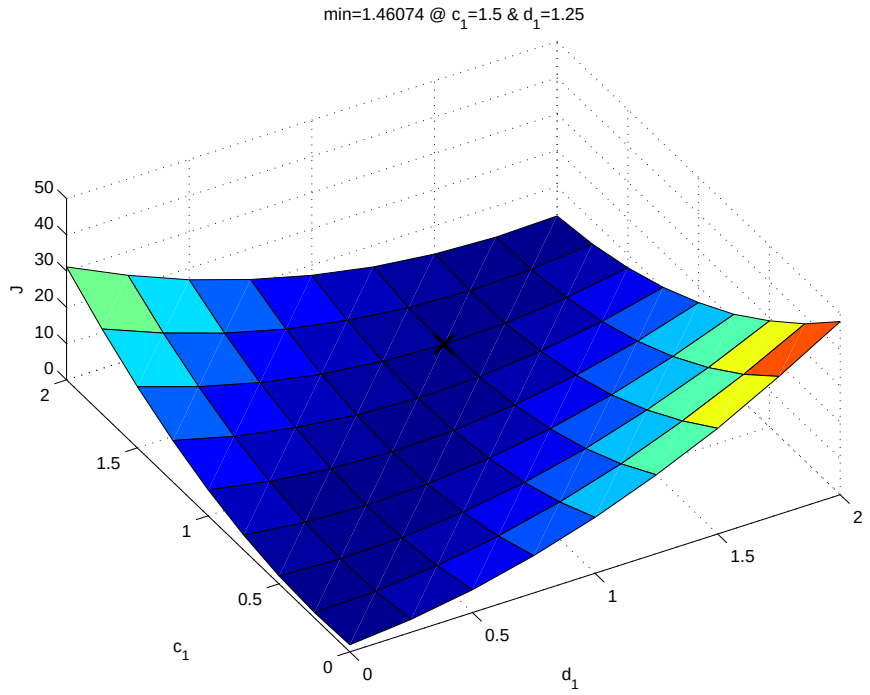

FIGURE 28. The relative cost, with all other distribution parameters constant, as c_1 and d_1 vary.

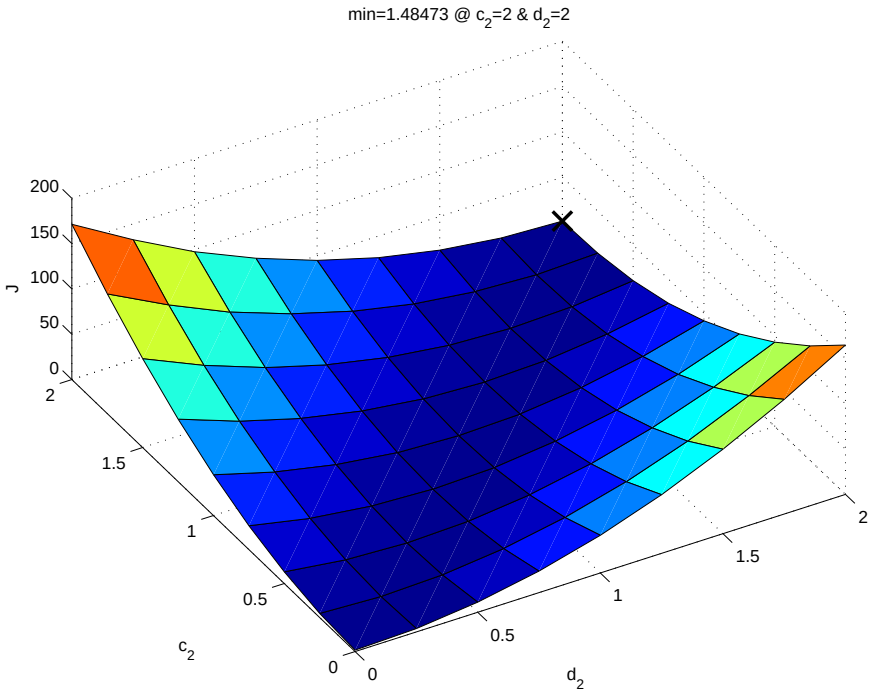

FIGURE 29. The relative cost, with all other distribution parameters constant, as c_2 and d_2 vary.

9. APPENDIX B

Appendix B uses the data retrieved in the eight parameter fit to true data. Each figure shows how the relative cost is affected by varying distribution parameters.

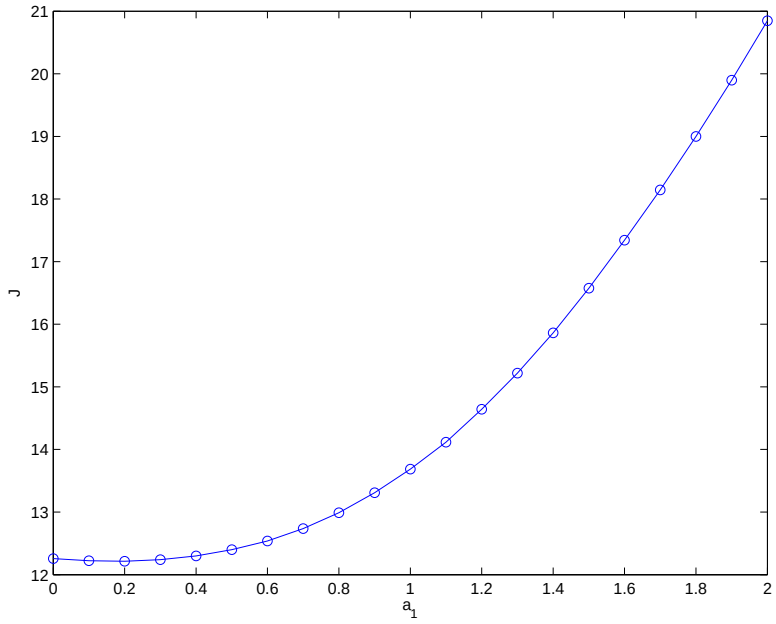

FIGURE 30. The relative cost, with all other distribution parameters constant, as a_1 varies.

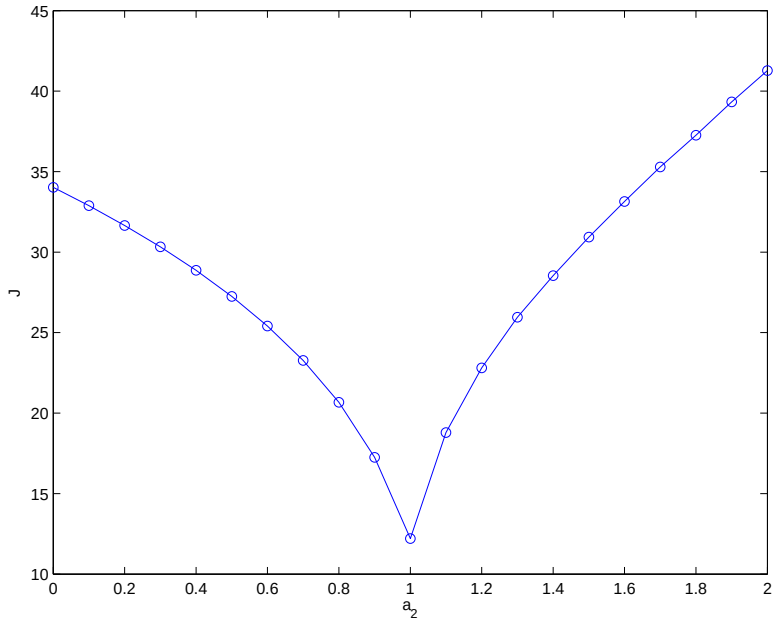

FIGURE 31. The relative cost, with all other distribution parameters constant, as a_2 varies.

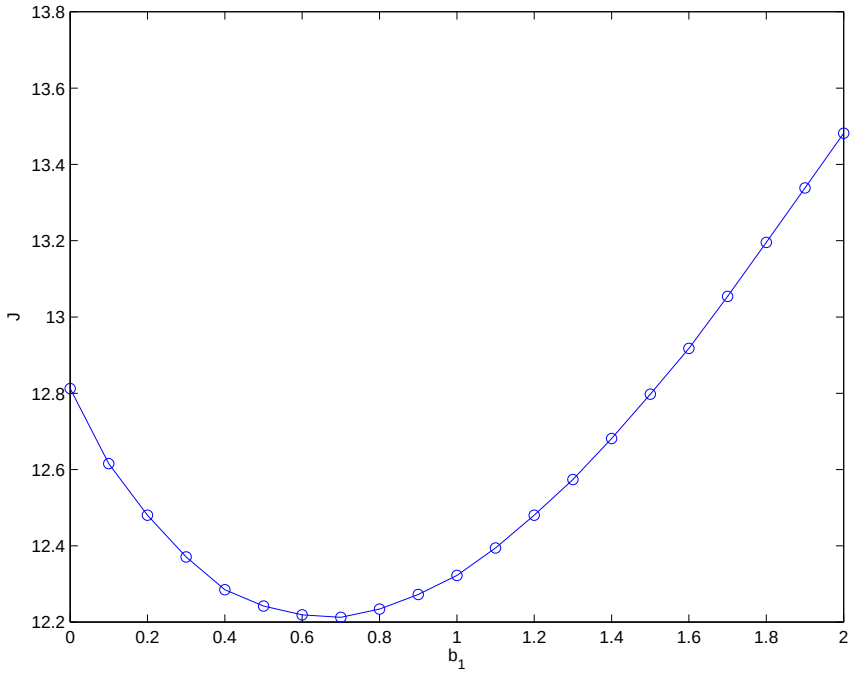

FIGURE 32. The relative cost, with all other distribution parameters constant, as b_1 varies.

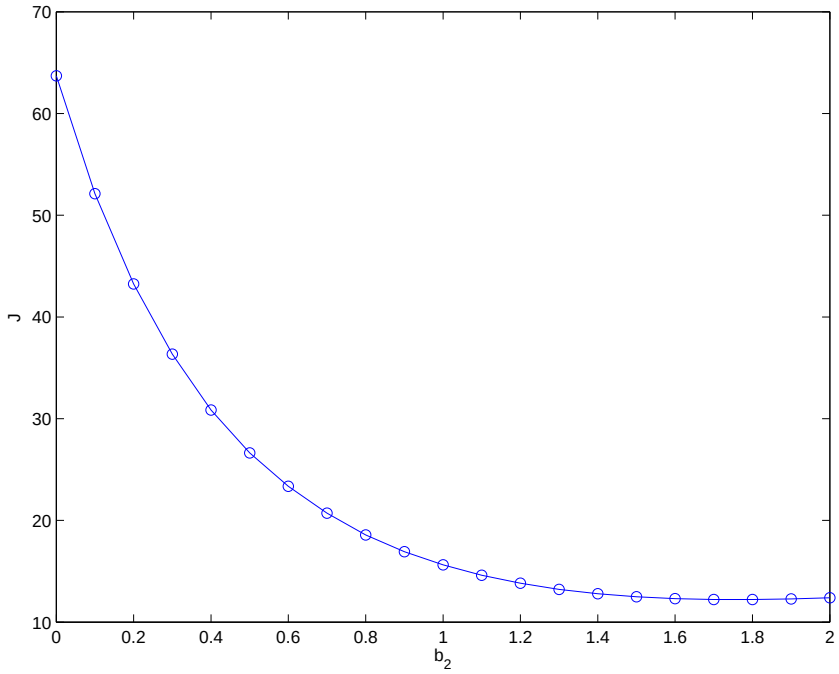

FIGURE 33. The relative cost, with all other distribution parameters constant, as b_2 varies.

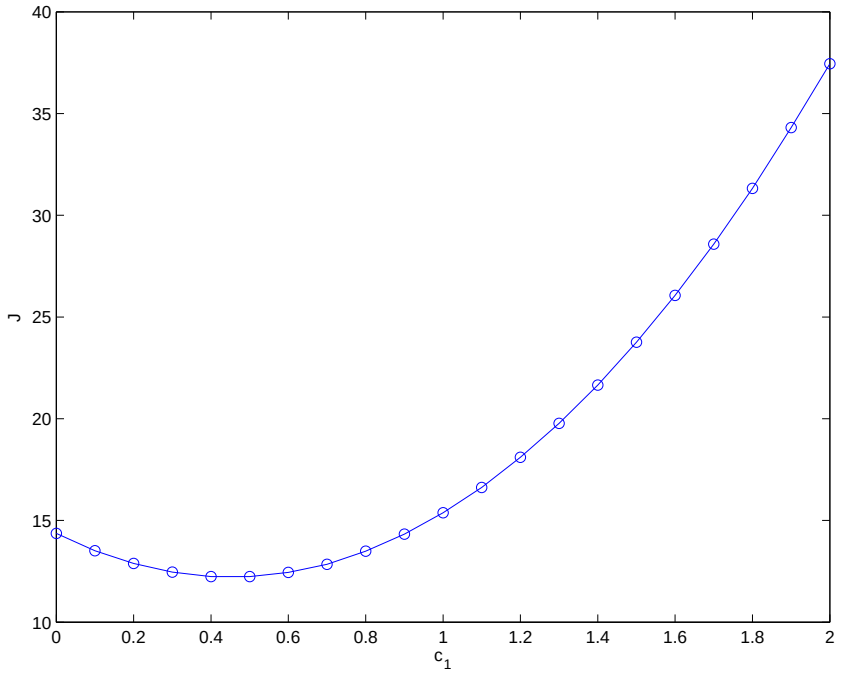

FIGURE 34. The relative cost, with all other distribution parameters constant, as c_1 varies.

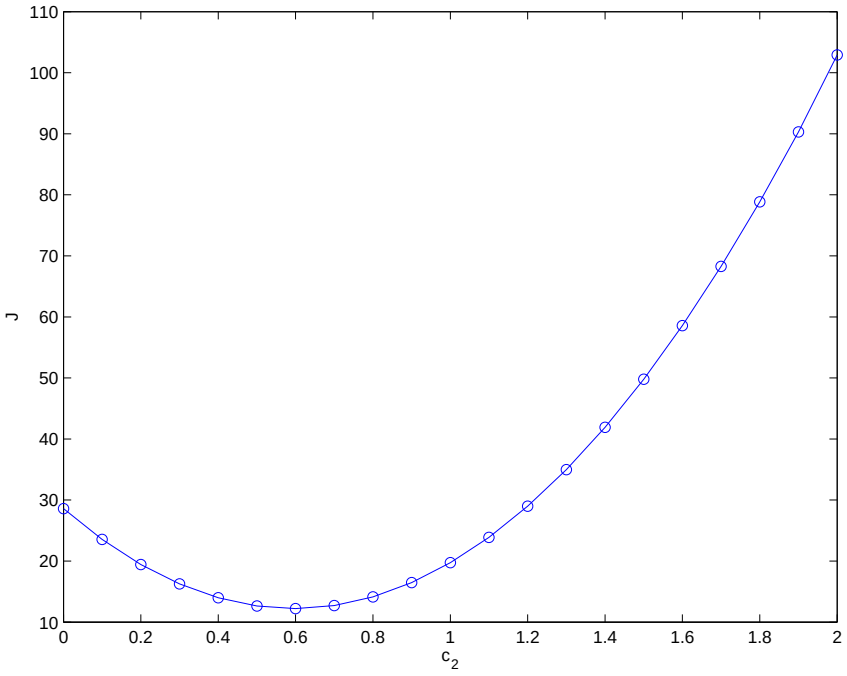

FIGURE 35. The relative cost, with all other distribution parameters constant, as c_2 varies.

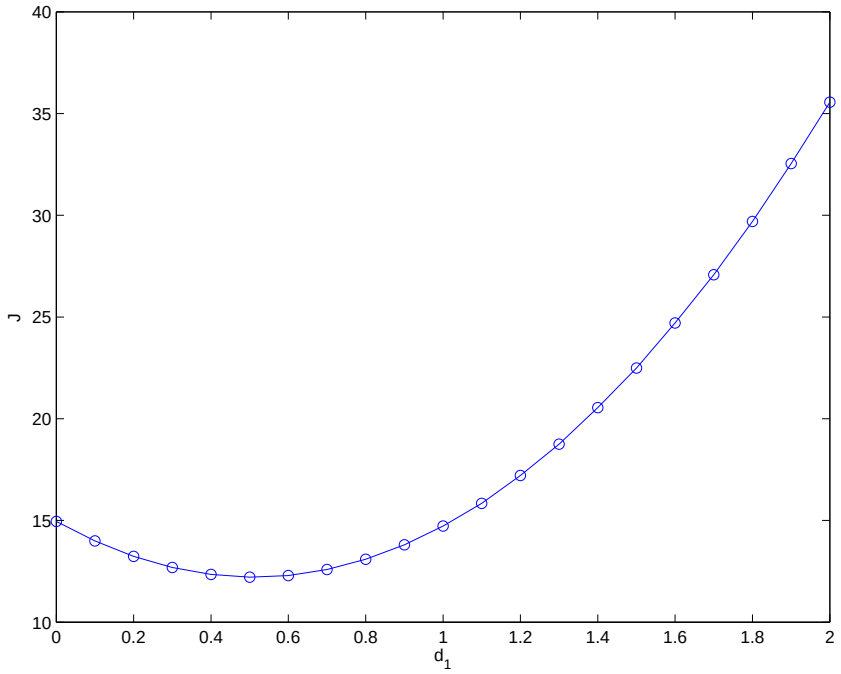

FIGURE 36. The relative cost, with all other distribution parameters constant, as d_1 varies.

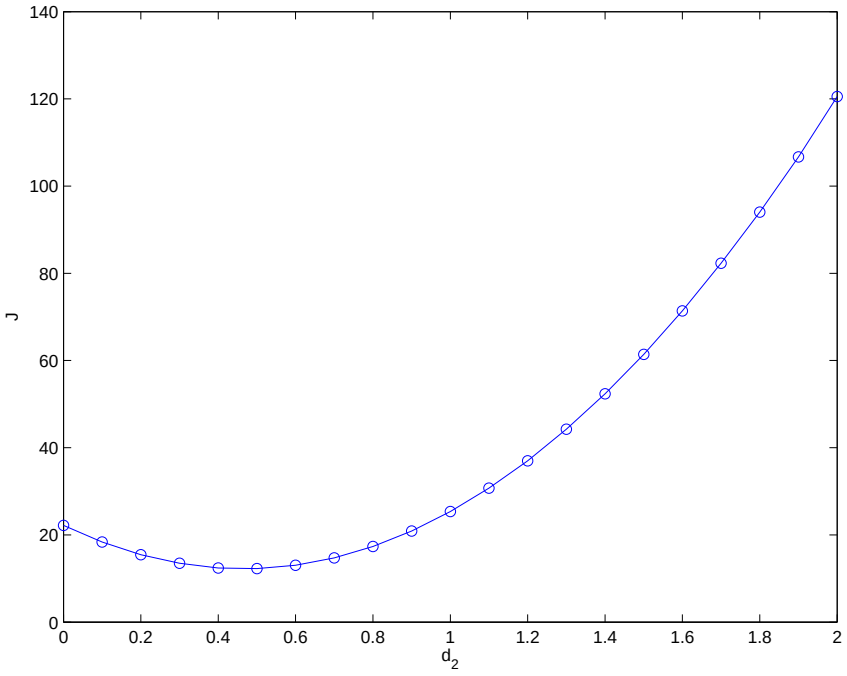

FIGURE 37. The relative cost, with all other distribution parameters constant, as d_2 varies.

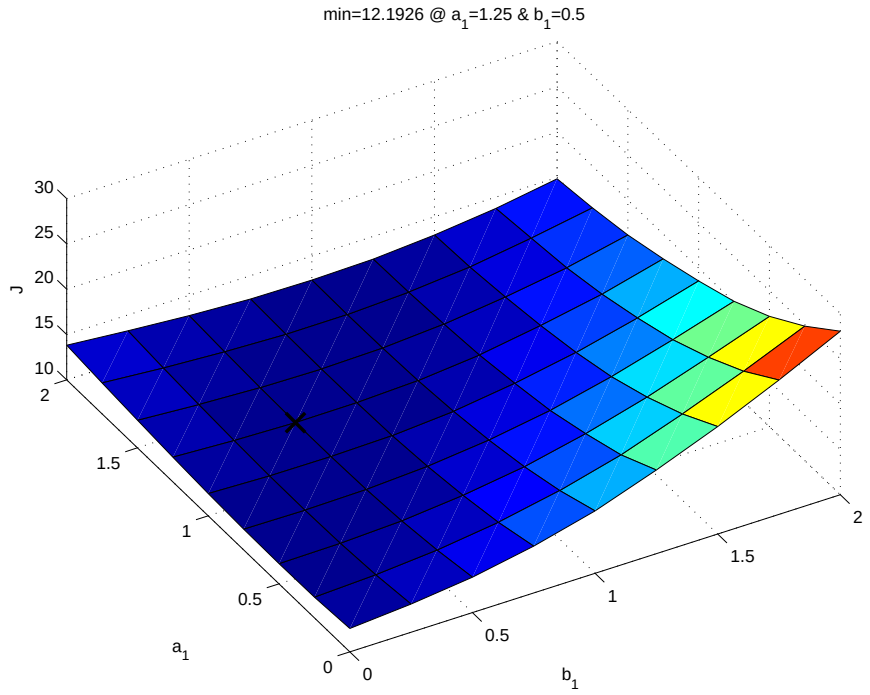

FIGURE 38. The relative cost, with all other distribution parameters constant, as a_1 and b_1 vary.

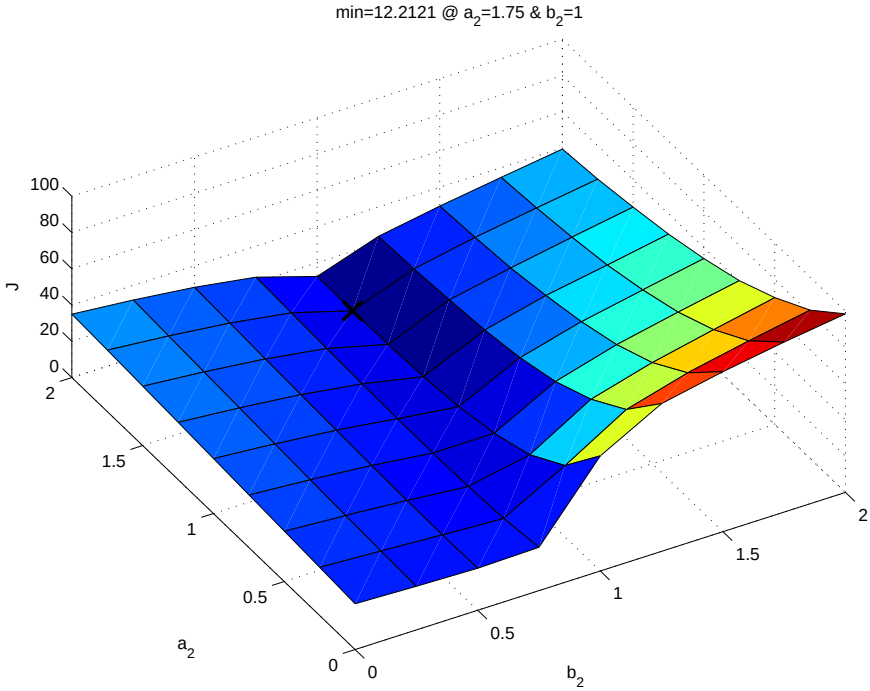

FIGURE 39. The relative cost, with all other distribution parameters constant, as a_2 and b_2 vary.

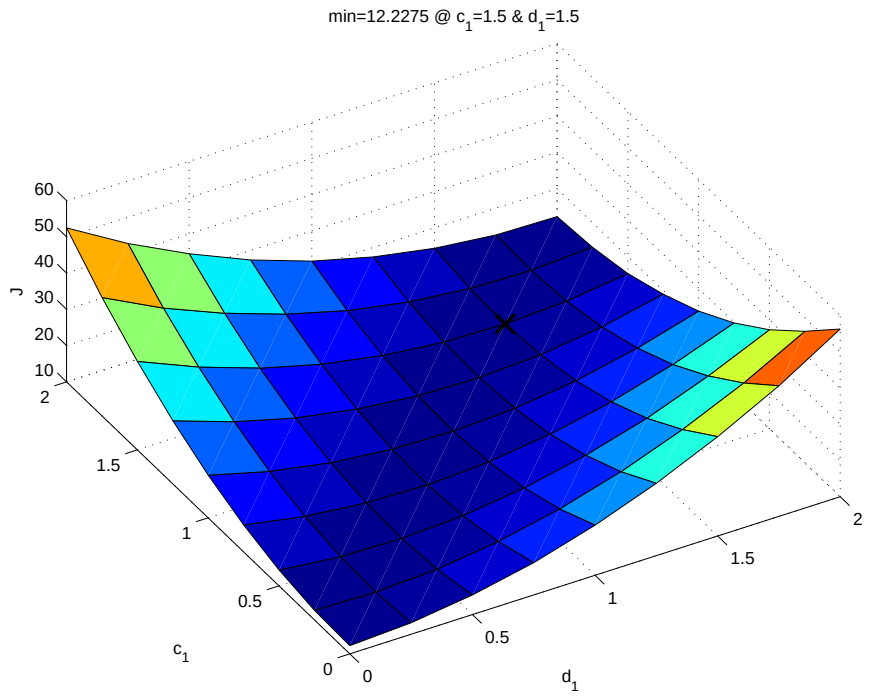

FIGURE 40. The relative cost, with all other distribution parameters constant, as c_1 and d_1 vary.

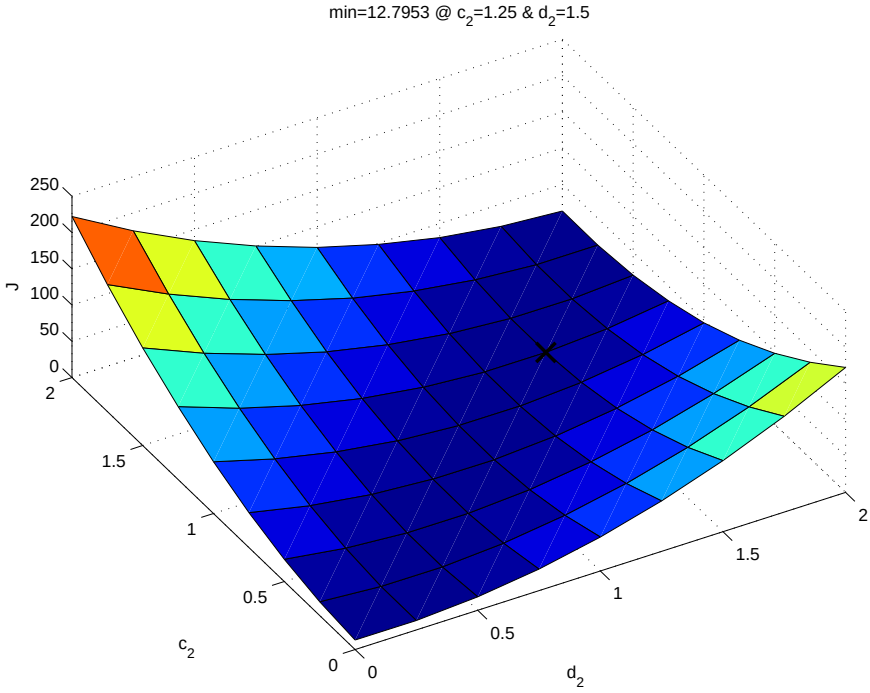

FIGURE 41. The relative cost, with all other distribution parameters constant, as c_2 and d_2 vary.

10. Appendix C

In Appendix C, we provide a figure similar to Figure 16. Here, the peak frequency occurs at 1×10^9(Hz) as opposed to 2×10^9(Hz).

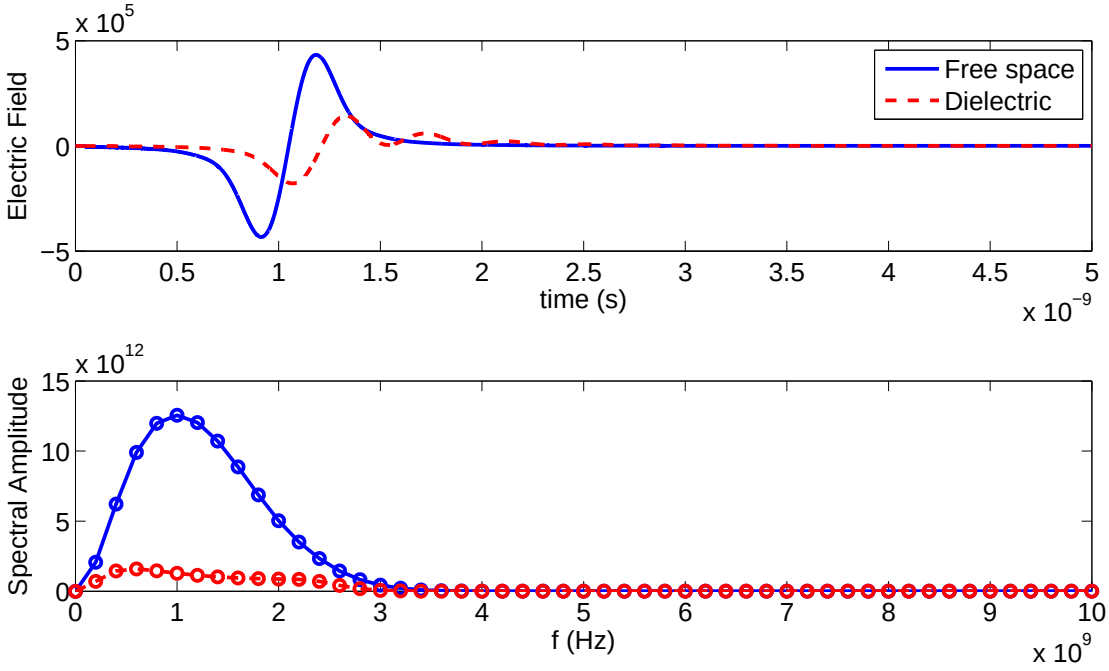

FIGURE 42. The top plot shows the value of the electric field at x=0.0155 as time varies. The dielectric begins at x=0.005 and ends at x=0.015. The bottom plot shows the FFT of the two signals.

REFERENCES

[1] HT Banks, MW Buksas, and T. Lin. *Electromagnetic Material Interrogation Using Conductive Interfaces and Acoustic Wavefronts*. Society for Industrial Mathematics, 2000.
[2] HT Banks and NL Gibson. Electromagnetic inverse problems involving distributions of dielectric mechanisms and parameters. *QUARTERLY OF APPLIED MATHEMATICS*, 64(4):749, 2006.
[3] C. J. F. Böttcher and P. Bordewijk. *Theory of Electric Polarization*, volume II. Elsevier, New York, 1978.
[4] K. Diethelm. An algorithm for the numerical solution of differential equations of fractional order. *Electronic Transactions on Numerical Analysis*, 5(1):6, 1997.
[5] D.E. Finkel. DIRECT Optimization Algorithm User Guide. *Center for Research in Scientific Computation North Carolina State University, Raleigh, NC*, pages 27695–8205, 2003.
[6] S. Gabriel, RW Lau, and C. Gabriel. The dielectric properties of biological tissues: III. Parametric models for the dielectric spectrum of tissues (results available online at http://niremf.ifac.cnr.it/docs/DIELECTRIC/home.html). *Phys. Med. Biol*, 41(11):2271–2293, 1996.
[7] JD Jackson. Classical Electromagnetics. *2nd eds. Wiley, New York*, 1975.
[8] CD Perttunen, DR Jones, and BE Stuckman. Lipschitzian optimization without the lipschitz constant. *Journal of Optimization Theory and Application*, 79(1):157–181, 1993.
[9] D.M. Sullivan. *Electromagnetic simulation using the FDTD method*. IEEE Press, New York, 2000.

OREGON STATE UNIVERSITY
E-mail address: barreska@onid.orst.edu

TUFTS UNIVERSITY
E-mail address: neel.chugh@tufts.edu